

2019

Qualitative and quantitative analysis of cortical type gradients in the human prefrontal cortex

<https://hdl.handle.net/2144/37012>

"Downloaded from OpenBU. Boston University's institutional repository."

BOSTON UNIVERSITY
SARGENT COLLEGE OF HEALTH AND REHABILITATION SCIENCES

Thesis

**QUALITATIVE AND QUANTITATIVE ANALYSIS OF CORTICAL TYPE
GRADIENTS IN THE HUMAN PREFRONTAL CORTEX**

by

JULIA LIAO HACKER

B.S., Boston University, 2018

Submitted in partial fulfillment of the
requirements for the degree of
Master of Science

2019

© 2019 by
JULIA LIAO HACKER
All rights reserved

Approved by

First Reader

Vasileios Zikopoulos, Ph.D.
Assistant Professor of Health Sciences

Second Reader

Miguel Á. García-Cabezas, Ph.D.
Research Assistant Professor of Health Sciences

ACKNOWLEDGMENTS

I would like to thank the donors of human brain tissue and their families for their generous contribution to research efforts. I would also like to thank the following people who have supported me along the way, not only during the course of this research, but throughout my combined Bachelor's and Master's degrees at Boston University.

I thank Dr. Zikopoulos and Dr. García-Cabezas for their patience, guidance, and instruction throughout the years and for the duration of this research project.

I would like to thank Tara McHugh, Iris Trutzer, Julied Fernanda Bautista Alvarez, Malavika Rangunathan, Nayeem Hossain, Ify Onochie, Shimrani Banik, Mary K. Joyce, Jinyi Wang, Yohan John, Xuefeng Liu, Marcia Feinberg, Helen Barbas, and Danka Charland for their invaluable advice and emotional support throughout this research project.

I would also like to thank my coworkers at the Science & Engineering Library, ScribeAmerica, and Boston University Residence Life for their patience and wisdom throughout this graduate degree.

I would be remiss not to thank the small Human Physiology graduate program cohort, including Sheshank Mageshwar, Jack Ganey, Jesse Moreira, Rachel Steiner, Kate Pinson, and Mandy Pinheiro, for the many laughs, shared experiences, and emotional support.

Lastly, I would like to thank my mother, Lingchin Liao; my sister, Mae Liao Hacker; and my greatest friend, Harry Lodes, for their endless love and support. It is with the support of my family that I am able to have this incredible experience.

**QUALITATIVE AND QUANTITATIVE ANALYSIS OF CORTICAL TYPE
GRADIENTS IN THE HUMAN PREFRONTAL CORTEX**

JULIA LIAO HACKER

ABSTRACT

The cerebral cortex, the outer part of the brain that has expanded in humans, has layers whose differentiation varies within gradients. Along those gradients, we can define cortical types which range in number of layers and degrees of laminar differentiation. From least to most elaborate types there is an increase in the presence of granular layer IV, a shift in relative prominence of deep (layers V–VI) to superficial layers (layers II–III), and shift in location of large pyramidal neurons from deep (layers V–VI) to superficial layers (layers II–III), an increase in differentiation of deep layers (layers V–VI), and an increase in a defined boundary between layers I–II. According to this criteria, the following cortical types were defined: agranular, dysgranular, eulaminate I, and eulaminate II. In addition, primary areas in the cerebral cortex show distinct cortical features and are named koniocortices. Prior studies have shown that cortical types are related to epigenetics, synaptic plasticity, connections, pathologies, and evolution.

Therefore, an algorithm to determine cortical type across areas in the human cortex will be a useful tool for the study of normal and pathological cortical networks. The Nissl stain, a standard histological staining method, was used in this study to observe differences in cortical type characteristics across the cerebral cortex. Qualitative analysis was performed on several cortical regions of an established neuroanatomical atlas, the prefrontal cortex of a post-mortem human, and the cerebral cortex of a rhesus macaque.

Five laminar features were identified and used to group cortical regions into types, with less than 5% of disagreement amongst at least three experienced neuroanatomists. From these cortical type characteristics, an algorithm was created that can be used to systematically to determine cortical type throughout the cerebral cortex of humans and rhesus macaques.

Additionally, quantitative analyses were performed in order to see if this cortical type classification could be an automated practice, that can be performed by individuals who are not experienced neuroanatomists. These quantitative measurements showed varying ability to classify cortical types; therefore, further studies will need to be performed in order to find the optimal quantitative measures of cortical type. A NMDS study was performed to summarize results of the various quantitative measurements, which showed an undisputable gradual trend of cortical types throughout the prefrontal cortex of the human brain. Overall, this study provides a cortical type classification algorithm that reliably and reproducibly identifies different cortical types in the cerebral cortex of human and rhesus macaque brains.

TABLE OF CONTENTS

ACKNOWLEDGMENTS	iv
ABSTRACT.....	v
TABLE OF CONTENTS.....	vii
LIST OF TABLES	ix
LIST OF FIGURES	xi
LIST OF ABBREVIATIONS.....	xiv
CHAPTER ONE: Introduction	1
CHAPTER TWO: Aims and Objectives.....	6
CHAPTER THREE: Methods	8
3.1 Experimental Design	8
3.2 Tissue acquisition and preparation	8
3.3 Staining	12
3.3.1 Nissl Staining	12
3.3.2 Immunohistochemistry	12
3.4 Qualitative Analysis by Light Microscopy	14
3.5 Cortical Type Classifications	15
3.5.1 Criteria for Cortical Type Classifications	15
3.5.2 Blinded and Unblinded Characterizations	21
3.6 Quantitative Analysis	25
3.6.1 Plot Profiles	25
3.6.2 Mean Gray Values	25

3.6.3 <i>Area Fractionation</i>	25
3.6.4 <i>Mean Pyramidal Neuron Sizes and Externopyramidization</i>	26
3.6.5 <i>Non-metric Multidimensional Scaling</i>	27
CHAPTER 4: Results	28
4.1 Qualitative Analysis	28
4.1.1 <i>Gross anatomy of the prefrontal cortex</i>	28
4.1.2 <i>Blinded and unblinded classifications displayed gradients of cortical types throughout the human and monkey cortex</i>	29
4.1.3 <i>SMI-32 Neurofilament Staining</i>	43
4.2 Quantitative Analysis	46
4.2.1 <i>Plot Profiles</i>	46
4.2.2 <i>Mean Gray Values</i>	50
4.2.3 <i>Area Fractionation</i>	53
4.2.4 <i>Mean Pyramidal Neuron Sizes and Ratio in Layers III and V</i>	57
4.2.5 <i>Non-metric Multidimensional Scaling</i>	61
CHAPTER FIVE: Discussion.....	63
CHAPTER SIX: Conclusions	68
BIBLIOGRAPHY.....	69
CURRICULUM VITAE.....	71

LIST OF TABLES

Table 1. Human Case Information Summary.....	10
Table 2. Characteristics of differential laminarity in human cortical types.....	19
Table 3. Characteristics of differential laminarity in rhesus macaque cortical type.....	20
Table 4. Cortical Type Classifications in the Frontal Lobe by von Economo/ Koskinas Areas.....	31–33
Table 5. Cortical Type Classifications in the Limbic Lobe by von Economo/ Koskinas Areas.....	34
Table 6. Cortical Type Classifications in the Insular Lobe by von Economo/ Koskinas Areas.....	35
Table 7. Cortical Type Classifications in the Parietal Lobe by von Economo/ Koskinas Areas.....	36–37
Table 8. Cortical Type Classifications in the Occipital Lobe by von Economo/ Koskinas Areas.....	37
Table 9. Cortical Type Classifications in the Temporal Lobe by von Economo/ Koskinas Areas.....	38
Table 10. Summary of assigned cortical types in the human cerebral cortex from the atlas of von Economo/Koskinas.....	39
Table 11. Summary of assigned cortical types in the PFC of human case HCD.....	41
Table 12. Summary of assigned cortical types in cerebral cortex of rhesus macaque case RAR.....	41

Table 13. Proposed scoring criteria for improved generalization of cortical type
classifications..... 67

LIST OF FIGURES

Figure 1. Human case HCD post-mortem left-hemisphere and block preparation.....	11
Figure 2. Regions of interest separated by cortical types in the anterior aspect of blocks 1–10 of human case HCD.....	17
Figure 3. Regions of interest separated by cortical types in the posterior aspect of blocks 1–10 of human case HCD.....	17
Figure 4. Regions of interest separated by cortical types in the anterior and posterior aspects of block 13 of human case HCD	18
Figure 5. Description of exclusion and inclusion criteria of pictures taken for human case HCD	18
Figure 6. Lateral aspect of human cortex.....	23
Figure 7. Processing and area parcellation of the lateral aspect of human case HCD in accordance to the atlas of von Economo.....	23
Figure 8. Medial aspect of human cortex.....	24
Figure 9. Processing and area parcellation of the medial aspect of human case HCD in accordance to the atlas of von Economo.....	24
Figure 10. Diagrams of human cerebral cortex by sulci and gyri, Brodmann areas (1909), and von Economo/Koskinas areas (1925/2008), from Mai et al. (2015).....	28
Figure 11. Comparison of cortical type distribution in human and rhesus macaque cortices	42
Figure 12. Comparison of SMI-32 and Nissl staining of the four cortical type in posterior block 10 of human case HCD	45

Figure 13. Representation of plot profile trends of the four cortical types spanning from the surface of the cortex to white matter in the prefrontal cortex of human case HCD	49
Figure 14. Averaged ratio of the upper half of plot profiles to the lower half of plot profiles, stratified by cortical type	49
Figure 15. Representation of plot profile trends of the cortical types spanning from the surface of the cortex to white matter of the prefrontal cortex in atlas of von Economo & Koskinas (1925/2018).....	50
Figure 16. Mean gray values for the Eulaminar II cortical type separated by orientations of medial, central, lateral, and ventral.....	51
Figure 17. Mean gray values for the Eulaminar I cortical type separated by orientations of medial, central, lateral, and ventral.....	52
Figure 18. Mean gray values for the Dysgranular cortical type separated by orientations of medial and ventral	52
Figure 19. Mean gray values for the Agranular cortical type separated by orientations of medial and ventral.....	53
Figure 20. Averaged area fractionation for layers III and V in four cortical types	54
Figure 21. Area fractionation for layers III and V in the Eulaminar II cortical type separated by orientations of medial, central, ventral, and lateral.....	55
Figure 22. Area fractionation for layers III and V in the Eulaminar I cortical type separated by orientations of medial, central, ventral, and lateral.....	56

Figure 23. Area fractionation for layers III and V in the Dysgranular cortical type separated by orientations of medial and ventral	57
Figure 24. Area fractionation for layers III and V in the Agranular cortical type separated by orientations of medial and ventral.....	57
Figure 25. Area fractionation for layers III and V in the varying cortical types separated by von Economo areas	58–59
Figure 26. Externopyramidization showing ratio of layers III to V in compared cortical areas stratified by cortical type	60
Figure 27. Averaged externopyramidization showing ratio of layers III to V in compared cortical areas stratified by cortical type	60
Figure 28. NMDS analysis of HCD-VE demonstrates expected trends by two methods of normalization	62

LIST OF ABBREVIATIONS

A/R/S.....	Age/Race/Sex
COD.....	Cause of Death
NDRI.....	National Disease Research Interchange
NMDS.....	Non-metric Multidimensional Scaling
PFC.....	Prefrontal cortex
PMI.....	Post-Mortem Interval
SMI-32.....	Sternberger-Meyer monoclonal antibody to a non-phosphorylated epitope on human NF-M and NF-H subunits of neurofilament protein

CHAPTER ONE: Introduction

A fundamental feature of cortical structure is that cortical neurons are arranged in layers. While common texts will refer to six cortical layers, classical architectonic maps of the cortex show that this is not always the case; cortical layers are not homogenous across the landscape of the brain (von Economo & Koskinas 1925/20018; Sanides 1962). Instead, cortical cytoarchitecture varies systemically in gradients from areas with fewer cortical layers to more elaborate areas with more cortical layers.

Limbic cortices, which contain the fewest number of cortical layers, are neocortical areas located on the outskirts of the hemisphere at the base of the cortex. Limbic cortices are further subdivided into either agranular (contain no layer IV) and dysgranular (contain a small and discontinuous layer IV). Eulaminate cortices, which contain the largest number of cortical layers, are neocortical areas with a thick, well-developed layer IV. Eulaminate cortices are further subdivided into either eulaminate I (equal prominence of layers III and V with no deep sublayers) or eulaminate II (prominence in layer III with presence of deep sublayers Va/b and VIa/b). Isocortex is another name for neocortical areas that have six layers, which is consistent with the criteria for a eulaminate area. Lastly, koniocortex is a very elaborate area that represents primary areas of the cortex, with a thick layer IV and a dense population of neurons and glia, such as the primary visual cortex (area 17), primary gustatory cortex (area 43), primary auditory cortex (area 41, 42), and primary somatosensory cortex (area 1, 2, 3). The primary motor cortex (area 4) has laminar differentiation comparable to koniocortices, but is poor in granule cells (García-Cabezas & Barbas 2014).

One hypothesis to explain the evolutionary origin of laminar gradients is the Dual Origin of the Neocortex, which proposes that cortical evolution occurs by several rings of cortex with increasing elaboration, beginning with a primitive ring connecting ancient olfactory cortex with ancestral hippocampal cortex. This hypothesis was independently proposed by Dart (1934), Abbie (1940, 1942), and Sanides (1962) based on findings across different species, and is essential to the understanding of cortical evolution. Recently, the Dual Origin of the Neocortex hypothesis has been supported by a causal explanation by the neurodevelopmental work of Puelles (2017, 2019), who showed that primitive ring formation is influenced by the opposing morphogenetic protein gradients of hem and anti-hem. From the primitive ring, gradients of laminar differentiation become more elaborated throughout neocortical expansion. The formation of cortical layers and gradients of laminar elaboration in the human cortex has been traced back to development (García-Cabezas *et al.* 2019).

Laminar gradients are essential to understand the organization of cortical networks and the flow of information in the cerebral cortex. Laminar patterns of connections are related to cortical structure, as elaborated in the Structural Model, which is based on the work of Barbas (Barbas 1986, Barbas & Rempel-Clover 1997) [reviewed in (García-Cabezas *et al.* 2019)] on bidirectional prefrontal connections in the monkey cortex. According to this model, connections from areas with lower laminar differentiation to areas with higher laminar differentiation originate in deep layers (layers V–VI) and terminate in superficial layers (layers I–III). In the reverse direction, from more elaborated areas to less elaborated areas, projections originate in superficial layers

(layers II–III) and terminate in middle/deep layers (IV–VI). Equally elaborate cortices (limbic to limbic or eulaminate to eulaminate) communicate by lateral projections that includes most layers. Also, the Structural Model relates systematic variation in cortical structure to expression of markers of synaptic plasticity, neuronal stability, and cellular stress (García-Cabezas *et al.* 2017). Limbic areas have higher expression of plasticity markers, while eulaminate areas have higher expression of stability markers.

Furthermore, markers of cellular stress, such as GFAP, have higher levels of expression in limbic than eulaminate areas. Altogether, limbic areas are shown to be more vulnerable to psychiatric and neurological disease than eulaminate areas.

Given the functional implications of gradients of laminar differentiation, there is a need for a way to systematically classify different cortical types across different areas of the cortex. To make any predictions about the functional implications of a cortical area, it is essential to call attention to the differences between cortical area and cortical type.

Cortical area is defined as a specific region that is functionally distinct, which can be shown by cellular and molecular markers (García-Cabezas *et al.* 2019). The most widely accepted map of the brain separated into distinct cortical areas is that of Brodmann (1909/1999). Brodmann created cortical maps of humans and monkeys with the intention to relate histology to phylogeny (Zilles & Amunts 2010). Brodmann concluded that architectonic parcellation of the human cortex would be best understood when related to brains of non-human primates. The map of Brodmann that is widely utilized today includes 43 cytoarchitectonic areas in the human cortex and approximately 30 areas in monkeys, with a few cortical areas omitted from human maps due to lack of homologous

areas shared with monkeys. Since the creation of Brodmann's map in 1909, many subsequent maps have been created with varying number of cortical areas. Both Vogt and Vogt (1919) and von Economo and Koskinas (1925/2008) created new maps with more cortical areas than Brodmann (1909/1999). Vogt and Vogt (1919) studied myeloarchitecture and subdivided many Brodmann areas due to differentiation observed in intracortical nerve fibers (Zilles & Amunts 2010). Von Economo and Koskinas developed a map with new ontology for ease of classification: first letter represents the respective lobe, second letter represents cytoarchitectonic type, and the third letter(s) represent specifications of that area or subarea.

Conversely, a cortical map following Brodmann's work, created by Bailey and von Bonin (1951), contained fewer cortical areas. Bailey and von Bonin (1951) attempted to apply Brodmann's cortical area map in a blinded fashion to randomized cortical areas and found that Brodmann's maps lacked observer independency, reproducibility, and objectivity (Zilles & Amunts 2010). Therefore, the map generated by Bailey and von Bonin (1951) included a few cortices rather than distinct areas, including agranular cortex, dysgranular cortex, a homotypical isocortex, and koniocortex. While Bailey and von Bonin (1951) were justified in stating that it is difficult to distinguish cortical area in a blinded fashion, the present study will examine how generalized cortical type can be identified. While cortical areas are plentiful and diverse in function, there is a small number of cortical types, including allocortex, isocortex, dysgranular, agranular, eulaminate I/II, and koniocortex. The purpose of this study is to determine a reliable method of classifying cortical types by Nissl-stained post-mortem human brain tissue and

plates of the atlas of von Economo and Koskinas (1925/2008), which will aid in future studies of plasticity, vulnerability to disease, epigenetics, and connections.

CHAPTER TWO: Aims and Objectives

The goal of this study was to qualitatively and quantitatively examine the gradients in laminar differentiation across the PFC and create a classification system for cortical types across different cortical areas. An established atlas by von Economo & Koskinas (1925/2008) was utilized to first identify the different types of cortex and how these cortical types change gradually across cortical areas and lobes of the brain. This established atlas showed scanned plates of cortex stained with Nissl, which provided visualization of somas (including nuclei and proximal cytoplasm). The PFC of a post-mortem human brain was then processed, stained with Nissl, and exhaustively analyzed by light microscopy. After identifying five major features of laminar differentiation for distinguishing cortical types in both the atlas and the human tissue, immunohistochemistry was performed for SMI-32 neurofilament staining as another means of showing laminar differentiation. Cortical type classifications were also juxtaposed to Nissl-stained rhesus macaque tissue to demonstrate evolutionary conservation and reliability of the proposed classification system.

Quantitative analysis was then performed on the human tissue to objectively assess if the assigned cortical types showed laminar differentiation by plot profile, mean gray value, and area fractionation. These analyses were performed to show that cortical type classification was not entirely subjective, but instead demonstrated differences that could be quantified. Finally, the prefrontal cortices of the atlas and the human tissue were compared based on shared qualitative cortical type classifications and quantitatively analyzed by mean pyramidal neuron size, externopyramidization, and non-metric multi-

dimensional scaling. The purpose of this comparative analysis was to show that cortical types were translational between a historical atlas and processed tissue.

CHAPTER THREE: Methods

3.1 Experimental Design

The experimental design of this study was essential to create a method to identify cortical types based on qualitative and quantitative analysis of Nissl-stained tissue. An established atlas by von Economo and Koskinas (1925/2008) and processed human tissue were examined in a sequential unblinded and blinded manner. The blinded qualitative analysis of these two datasets allowed for five cortical type characteristics to be elucidated, including: existence of layer IV, relative prominence of superficial versus deep layers, largest pyramidal neurons, differentiation of layers V–VI, and state of boundary between layers I–II. A subsequent unblinded analysis allowed for re-examination of the blinded classifications with the added comprehension of topology, or the location of the examined cortical area within the cortex. Defining cortical types qualitatively allowed for further quantitative measures of the human tissue by ImageJ, which included plot profiles, mean gray value, and area fractionation. Comparative analysis between the prefrontal cortices of the atlas and of the human tissue allowed for quantitative measures of mean pyramidal neuron size, externopyramidization, and non-metric multidimensional scaling.

3.2 Tissue acquisition and preparation

Whole neurotypical post-mortem human brains were donated from the National Disease Research Interchange (NDRI) and from the Neuroanatomy Instructional Lab at Boston University's Sargent College of Health and Rehabilitation Sciences. Human

subjects were chosen and matched based on tissue availability. Post-mortem human brains were kept well-preserved and had low post-mortem intervals (PMI), with average PMI < 24h. The cerebellum and brainstem were completely resected from the cerebral cortex of the whole neurotypical post-mortem human brain. A macro dissection knife was then used to hemisect the whole cerebrum through the corpus callosum. Each hemisphere was cut into slabs of tissue approximately 2cm in thickness. These slabs of human brain were then blocked into smaller pieces based on various regions of interest (ROIs). Tissue blocks were frozen in methylbutane at -70°C prior to using a freezing microtome (Precisionary VF-700, Precisionary Instruments Inc., Grenville, NC, USA; Physitemp BFS-40MP Controller) to cut the tissue in the coronal plane into 10 series of 50 µm-thick sections. Photographs were taken of each section. Brain tissue was fixed in 10% formalin, cryoprotected in 30% sucrose, and stored at -20°C in anti-freeze solution (30% ethylene glycol, 30% glycerol, and 40% 0.05M phosphate buffer with 0.05% sodium azide). One section per series was placed aside in six-well plates filled with 0.1 phosphate buffer (pH 7.35) and subsequently mounted onto gelatin-coated slides (Gelatin Type A, G8-500, Fisher Scientific, Fair Lawn, New Jersey, US) to represent serial sectioning throughout the block. These mounted slides were given approximately ten days to dry prior to further staining.

Cases HCD, HAW, HAY, and HCP were used for immunohistochemical analysis of laminarity of cortical columns with SMI-32 anti-neurofilament. Brain tissue from Case HCD was primarily used for extensive brightfield imaging. Clinical characteristics on the human subjects are found summarized in Table 1.

<u>Case Number</u>	<u>A/R/S</u>	<u>Condition</u>	<u>PMI (h)</u>	<u>COD</u>	<u>Donor</u>
HCD	38/C/M	CTRL	18.9	Cardiac arrest	NDRI
HCP	55/C/M	CTRL	16.0	Cardiac arrest	NDRI
HAW 2758	58/C/F	CTRL	-	Pancreatic Cancer	NeuroAnat
HAY 3176	67/C/F	CTRL	-	Pancreatic Cancer	NeuroAnat

Table 1. Human Case Information Summary

A/R/S: Age/Race/Sex; PMI: post-mortem interval; COD: cause of death

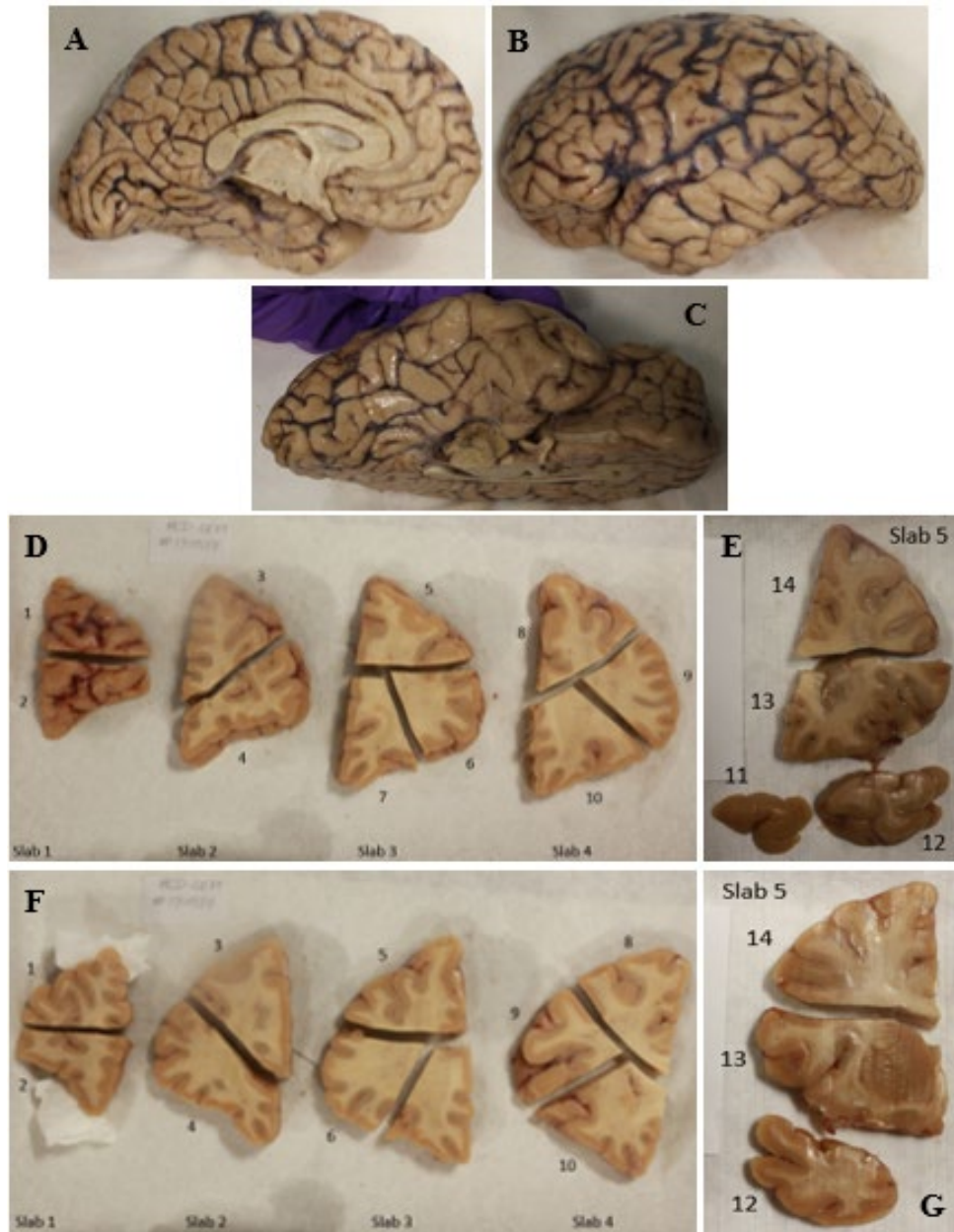


Figure 1. Human case HCD post-mortem left-hemisphere and block preparation (A) Medial View of Left Hemisphere **(B)** Lateral View of Left Hemisphere **(C)** Ventral View of Left Hemisphere **(D)** Anterior aspect of Slabs 1–4 separated into Blocks 1–10 **(E)** Anterior aspect of Slab 5 separated into Blocks 11–14 **(F)** Posterior aspect of Slabs 1–4 separated into Blocks 1–10 **(G)** Posterior aspect of Slab 5 separated into Blocks 12–14

3.3 Staining

3.3.1 Nissl Staining

To examine the gradients of laminarity in the cytoarchitecture of the PFC, especially pyramidal cell bodies in layers III and V, both human and monkey sections were stained with Nissl, which stains all soma of neurons and glia. The dry, mounted sections were placed in a 1:1 solution of chloroform (C298-1, Fisher Scientific) and 100% ethanol (Pharmco-AAPER, Brookfield, Connecticut, US) for a brief 2–3h period of de-fatting. After the de-fatting process, the sections were rehydrated using a gradient of 2-minute sessions of submersion in 100%, 95%, and 70% ethanol solutions and deionized water. The sections were then exposed to 0.05% thionin (pH 4.5) blue solution for 15 minutes. The sections were dehydrated using a gradient of 2-minute sessions of submersion in deionized water and 70%, 95%, and 100% ethanol solutions. During the first submersion bath of 95% ethanol, approximately 1 mL of acetone was applied to the sections to remove excess thionin blue solution from the tissue. After the dehydration process, sections were then submerged in xylenes (UN1307, Fisher Scientific) for approximately 45 minutes and coverslipped with Entellan (Merck, Whitehouse, New Jersey, US).

3.3.2 Immunohistochemistry

Both human and monkey tissue were processed with immunohistochemical methods to observe laminar distributions of pyramidal neurons within cortical columns with SMI-32 mouse anti-neurofilament H. SMI-32 was used to show the soma and

proximal dendritic processes of pyramidal neurons in deep layer III and superficial layer V, with no stained neurons in layer IV. Free-floating tissue was washed in 0.1M phosphate buffer (pH 7.35) for 5 minutes at 4°C prior to inactivation by endogenous peroxidase (1.5% H₂O₂ in 0.1M PB, pH 7.35) at 4°C. These sections were then washed with 0.1 phosphate buffer (pH 7.35) at 4°C. Sections were first washed with 10mM sodium citrate buffer (pH 8.5) at room temperature for 5 minutes prior to an antigen retrieval of tissue in a heated deionized water bath at 80°C. An antigen retrieval method was utilized as part of this immunohistochemical procedure in order to cleave existing methylene bridges that may have formed during fixation. By cleaving these methylene bridges, antibodies have a higher probability of binding to antigen sites.

Sections were washed with 0.1 phosphate buffer (pH 7.35) at 4°C and incubated in 50mM glycine (pH 7.35) at 4°C to inhibit unreacted aldehydes. After another round of washing with 0.1 phosphate buffer (pH 7.35) at 4°C, sections were placed in a preincubation solution (20% bovine serum albumin, 2% bovine serum albumin-C, 20% normal goat serum, 0.2% Triton-100 in 0.1 phosphate buffer (pH 7.35)) for 60 minutes at 4°C. Sections were then incubated in solution containing primary mouse anti-neurofilament H (20% bovine serum albumin, 2% bovine serum albumin-C, 20% normal goat serum, 0.1% Triton-100 in 0.1 phosphate buffer (pH 7.35)) for two nights in the dark at 4°C. Sections were placed in the BioWave microwave at 150W for 8 minutes prior to dark incubation.

Following the two nights of dark incubation at 4°C, the sections were placed in the BioWave microwave at 150W for 6 minutes. After washing the sections in 0.1

phosphate buffer (pH 7.35) at 4°C, sections were placed in secondary antibody solution (20% bovine serum albumin, 2% bovine serum albumin-C, 20% normal goat serum, 0.1% Triton-100 in 0.1 phosphate buffer (pH 7.35)) containing Biotynilated goat anti-mouse (Vector) for three and a half hours in the dark at room temperature. Sections were microwaved at 150W for 6 minutes at the beginning of incubation, and microwaved at 150W for 3 minutes at about halfway through the incubation period. After washing the sections with 0.1 phosphate buffer (pH 7.35) at 4°C, an avidin-biotin complex (Vector ABC kit, Vector Labs, Burlingame, CA) was applied to the sections for a 30-minute incubation in the dark at room temperature. Sections were microwaved at 150W for 5 minutes at both the beginning of incubation and halfway through the incubation period. The sections were then copiously washed with 0.1 phosphate buffer (pH 7.35) at 4°C. Sections were then placed in a solution containing 0.05% 3,3'-diaminobenzidine (DAB) and 0.03% hydrogen peroxide in 0.1M phosphate buffer (pH7.35) for 1–2 minutes by controlled development under a microscope. After DAB development, sections were washed with 0.1 phosphate buffer (pH 7.35), mounted on gelatin-coated slides (Gelatin Type A, G8-500, Fisher Scientific, Fair Lawn, New Jersey, US), and coverslipped with Entellan (Merck, Whitehouse, New Jersey, US) (Campbell & Morrison 1989, Trutzer *et al.* 2019).

3.4 Qualitative Analysis by Light Microscopy

Quantitative and qualitative analysis of the cyto- and myeloarchitecture of the gray matter of the PFC was performed at high resolution via brightfield microscopy at 10x, with pictures taken by CCD camera (Olympus DP70 Digital Camera System)

connected to an Olympus Fluorescent Microscope (BX51). Multiple images were taken with a preserved 5–10% overlap between images and photomerged in Adobe Photoshop.

This study includes an exhaustive analysis of the PFC of human case HCD. Figures 2–4 show the locations of regions of interest (ROIs) throughout the PFC, by the anterior aspect of blocks 1–10 (Figure 2), the posterior aspect of blocks 1–10 (Figure 3), and both anterior and posterior aspects of block 13 (Figure 4). Each ROI shown in Figures 2–4 has a label for its cortical type, with the key provided on each figure: red areas are eulaminar II, green areas eulaminar I, brown areas are dysgranular, purple areas are agranular, and blue areas are either curved or damaged areas.

In total, 482 pictures were taken of Nissl-stained cortical columns by light microscopy. For further qualitative and quantitative analysis, 311 of the original 482 were utilized while the remaining 171 were excluded. Exclusion criteria included: presence of a deep invagination consistent with a sulcus (n=83); overlap of layer I with an adjacent tissue without clear distinction (n=16); mild layer I tissue damage by stain or processing (n=58); and miscellaneous reasons of bad staining or extensive damage by stain or processing (n=14). This is summarized in Figure 5.

3.5 Cortical Type Classifications

3.5.1 Criteria for Cortical Type Classifications

Strict parameters and inclusion criteria were defined for cytoarchitectonic classifications dependent on degree of laminarity. Three basic divisions were created to describe degree of laminarity from most rudimentary to most elaborate: limbic,

eulamine, and koniocortex. These three overarching categories were separated into smaller subdivisions. Limbic branched into agranular and dysgranular; eulamine branched into eulamine I and II; and koniocortex was used to identify primary cortical areas, such as primary motor (area 4), primary visual (area 17), and primary auditory cortices (area 41/42). Criteria for these four subdivisions included several structural characteristics of these cortical areas, which were visualized by Nissl staining. Characteristics included existence of layer IV; relative prominence of superficial versus deep layers, largest pyramidal neuron sizes, differentiation between layers V and IV, and state of the boundary between layer I and II. Table 2 shows characteristics of different cortical area classifications, as a gradient from limbic (e.g. agranular, dysgranular) to neocortical areas (e.g. eulamine I/II/II, koniocortex).

These cortical type characteristics were then applied to Nissl-stained rhesus macaque cortical areas for qualitative comparison. These rhesus macaque brains were not processed during the duration of this study or for the purpose of this study. Rhesus macaque brains were archival tissue that was previously obtained, processed, cut, stained with Nissl, coverslipped, and analyzed with light microscopy in a similar fashion to the human tissue processing detailed in this study. Adjusted cortical types characteristics are summarized in Table 3.

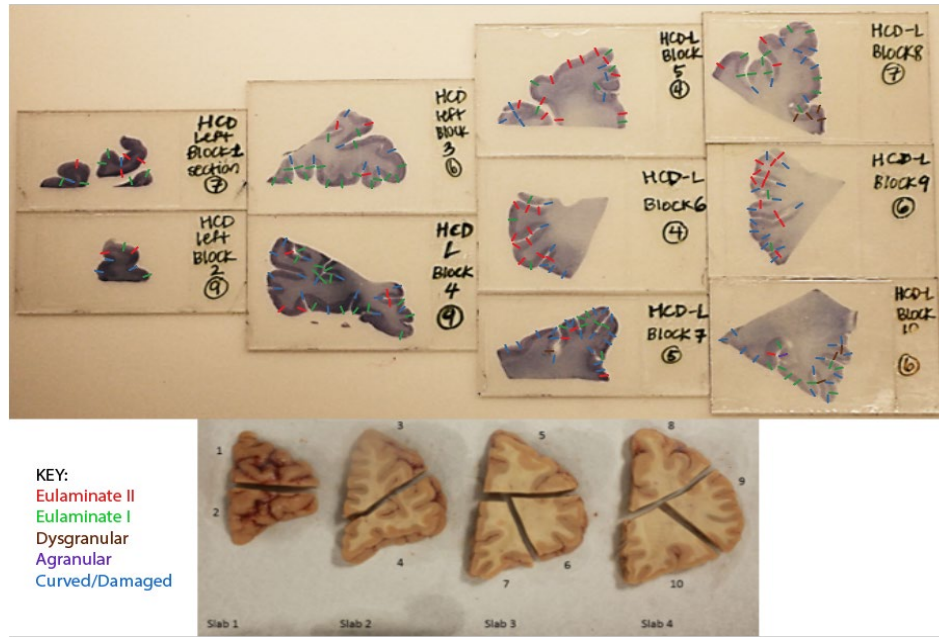


Figure 2. Regions of interest separated by cortical types in the anterior aspect of blocks 1–10 of human case HCD

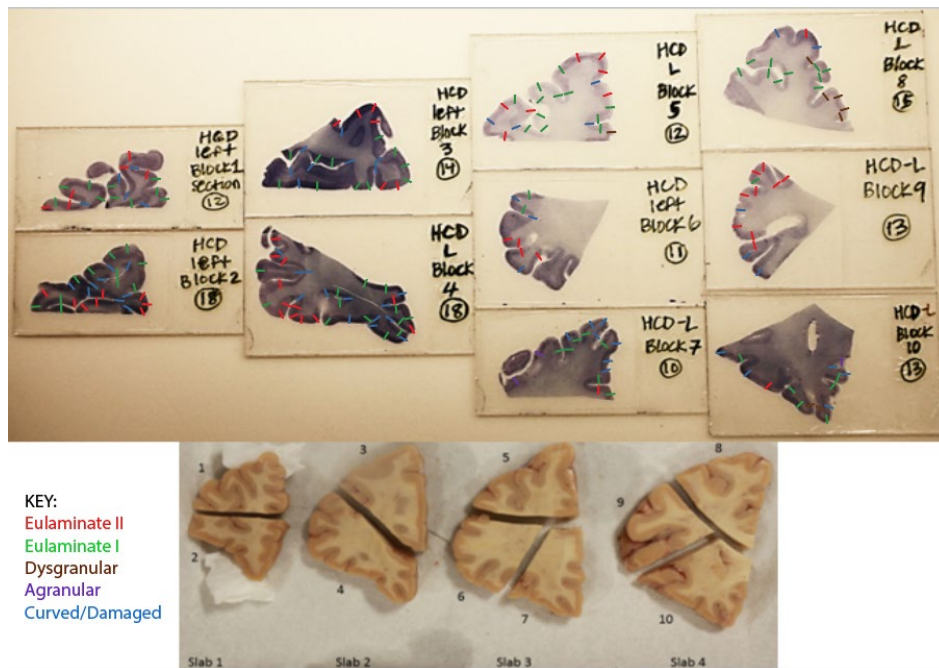


Figure 3. Regions of interest separated by cortical types in the posterior aspect of blocks 1–10 of human case HCD

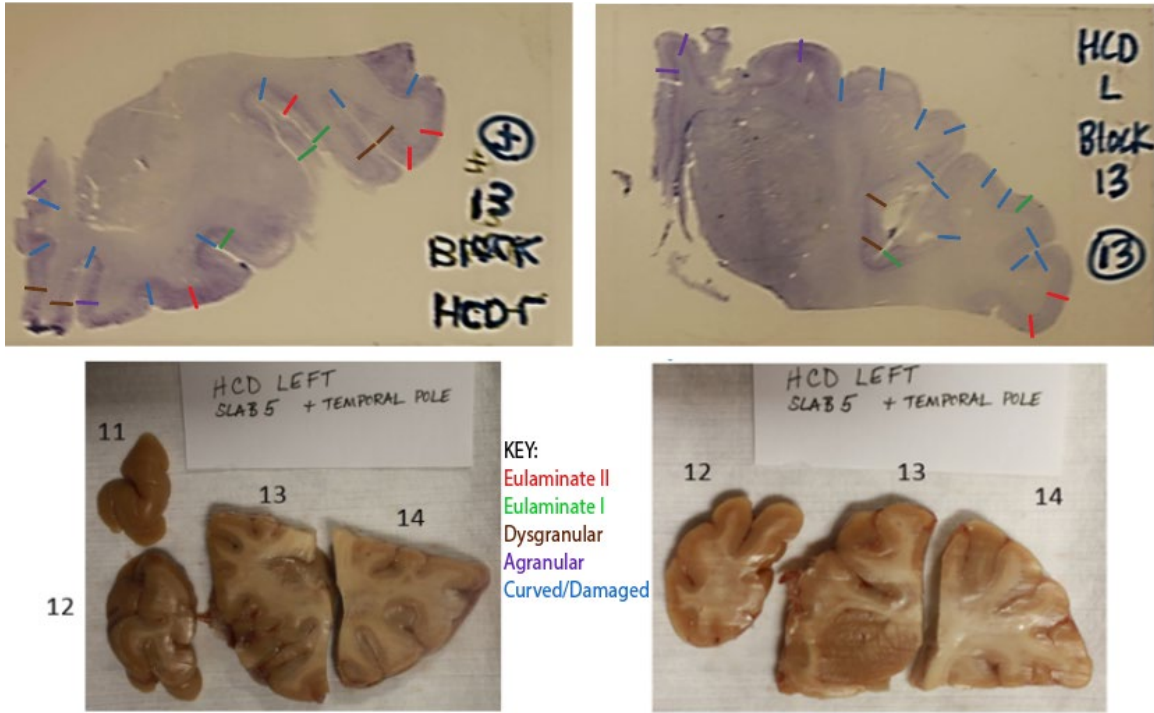


Figure 4. Regions of interest separated by cortical types in the anterior and posterior aspects of block 13 of human case HCD

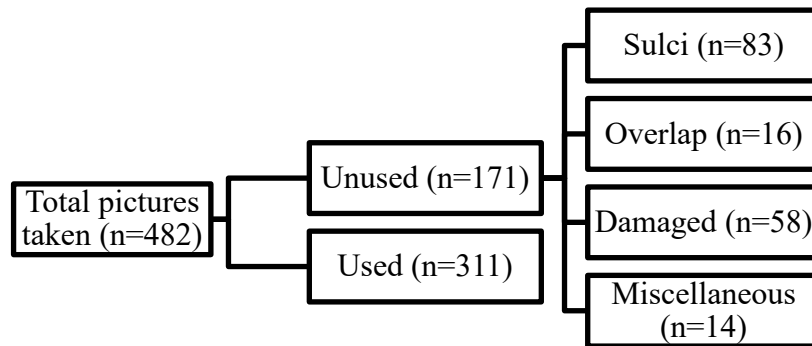


Figure 5. Description of exclusion and inclusion criteria of pictures taken for human case HCD

<u>Characteristics</u>	CORTICAL TYPES				
	<i>LIMBIC</i>		<i>EULAMINATE</i>		<i>PRIMARY CORTICAL AREAS</i>
	<u>A-granular</u>	<u>Dys-granular</u>	<u>Eulaminate I/ Premotor I</u>	<u>Eulaminate II/ Premotor II</u>	<u>Koniocortex/ Primary Motor</u>
Existence of Layer IV	Absent	Thin, irregular, discontinuous	Thin, regular, continuous	Thick, regular, continuous	Thick, regular, continuous
Relative prominence of Superficial versus Deep Layers	Deep (Layers V–VI)	Deep (Layers V–VI)	Equal; Deep (Layers V–VI) & Superficial (Layers II–III)	Superficial (Layers II–III)	Superficial (Layers II–III); Higher density of small neurons
Largest pyramidal neurons	Layer V	Layer V	Both Layer V & III	Layer III	Layer III; Presence of Betz cells in Layer V of Primary Motor
Differentiation of Layers V–VI	Poor	Poor; present in cingulate	Improved presence of sublayers	Presence of clear sublayers	Presence of clear sublayers
State of boundary between Layers I–II	Irregular; not consistent	Slight irregularities	Sharp	Sharp	Sharp

Table 2. Characteristics of differential laminarity in human cortical types

<u>Characteristics</u>	CORTICAL TYPES				
	<i>LIMBIC</i>		<i>EULAMINATE</i>		<i>PRIMARY CORTICAL AREAS</i>
	<u>A-granular</u>	<u>Dys-granular</u>	<u>Eulaminate I/ Premotor I</u>	<u>Eulaminate II/ Premotor II</u>	<u>Koniocortex/ Primary Motor</u>
Existence of Layer IV	Absent	Thin, irregular, discontinuous	Thin, regular, continuous; Not visible by Nissl stains in Premotor I	Thick, regular, continuous; Not visible by Nissl stains in Premotor II	Thick, regular, continuous; Not visible by Nissl stains in Primary Motor
Relative prominence of Superficial versus Deep Layers	Deep (Layers V–VI)	Deep (Layers V–VI)	Equal; Deep (Layers V–VI) & Superficial (Layers II–III)	Superficial (Layers II–III)	Superficial (Layers II–III); Higher density of small neurons
Largest pyramidal neurons	Layer V	Layer V	Both Layer V & III	Layer III	Layer III
Differentiation of Layers V–VI	Poor	Poor	Improved presence of sublayers	Presence of clear sublayers	Presence of clear sublayers
State of boundary between Layers I–II	Irregular; not consistent	Slight irregularities	Sharp	Sharp	Sharp

Table 3. Characteristics of differential laminarity in rhesus macaque cortical types

3.5.2 Blinded and Unblinded Characterizations

The atlas of von Economo and Koskinas (1925/2008) provided high-quality pictures of Nissl stained sections of cortical areas. These sections, or plates, as they are referred to in the original text, were scanned and printed without indication of the area previously determined by von Economo. These printed copies of the plates were randomized, and a blind classification was performed based on the criteria summarized in Table 2. After this blinded classification, an unblinded classification was performed to ensure the cortical type classifications made topological sense.

Areas demarcated by von Economo/Koskinas (1925/2008), or VE areas, were then directly compared with pictures taken of human case HCD. Sulci and gyri were compared between these two cortical maps to identify VE areas on the lateral (Figures 6, 7) and medial (Figures 8, 9) surfaces of the hemi-sectioned brain of human case HCD. Figures 6 and 8 show juxtaposition of the map of VE areas provided by the atlas of von Economo and Koskinas (1925/2008) to the lateral and medial surfaces of human case HCD respectively. Figures 7 and 9 show where and how PFC was slabbed and blocked in relation to VE areas of the lateral and medial surfaces of human case HCD, respectively. Once these VE areas were identified on the surface of the human case HCD cortex, every picture that was taken (n=482) of human case HCD was assigned a VE area in one of four orientations depending on location: medial, lateral, ventral, and central. Assigning VE area designations to the human case HCD cortical columns showed that the utilized PFC pictures belonged to 31 different VE areas.

Therefore, one picture of the PFC in human case HCD was chosen to best

represent each of these prefrontal VE areas (n=31). Selecting these 31 pictures provided a way to directly compare the prefrontal cortices of the atlas of von Economo and Koskinas (1925/2008) and of the human case HCD. These 31 comparison pictures, or ‘HCD-VE’ as they will be referred to henceforth, were used to show how cortical type classifications are translational from a nearly century-old atlas of the human cortex to a current, tangible post-mortem brain that was processed at the beginning of this study.

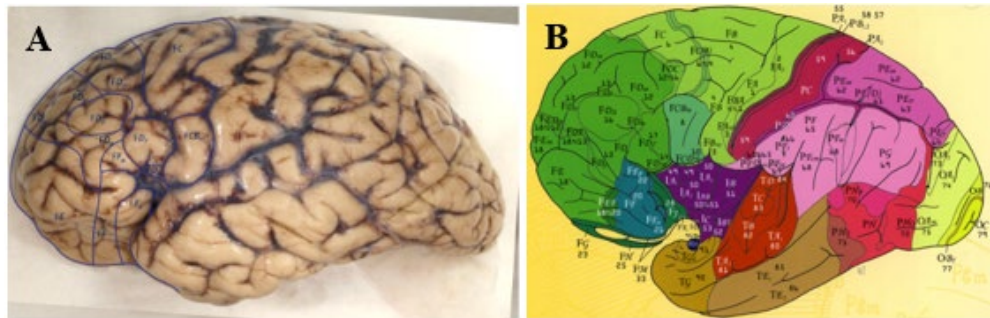


Figure 6. Lateral aspect of human cortex A) Lateral aspect of human case HCD with demarcations of areas established by von Economo. B) Lateral aspect of human cortex provided by the atlas of von Economo & Koskinas (1925/20018)

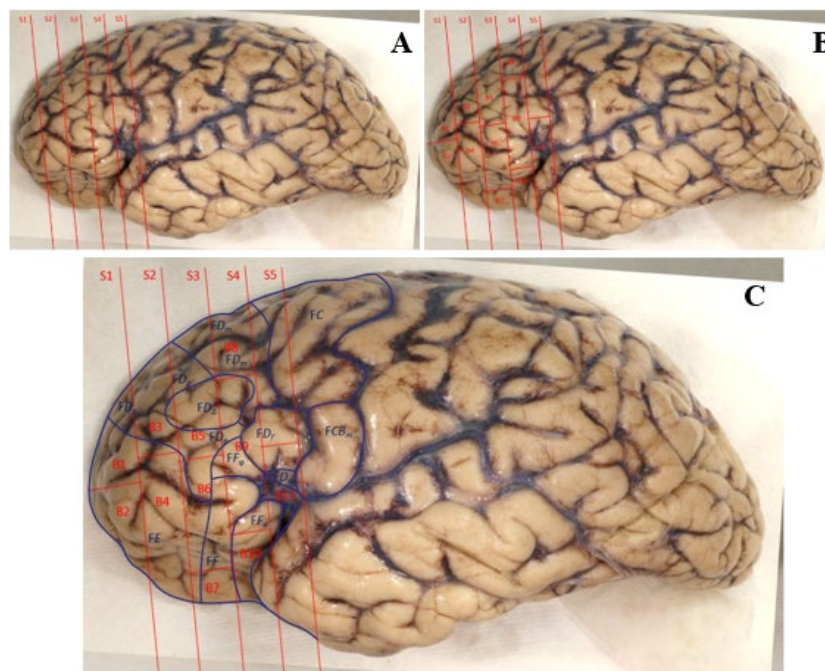


Figure 7. Processing and area parcellation of the lateral aspect of human case HCD in accordance to the atlas of von Economo A) Lateral aspect of human case HCD separated into 5 slabs of PFC. B) Lateral aspect of human case HCD separated into multiple blocks within 5 slabs of PFC. C) Lateral aspect of human case HCD separated into slabs and blocks with overlying von Economo area demarcations.

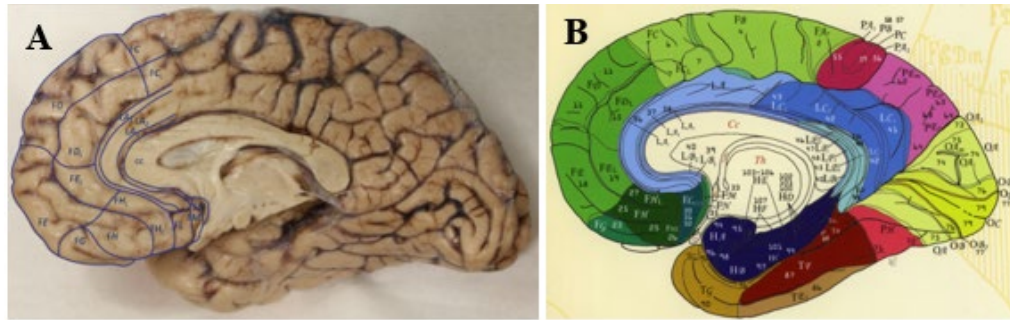


Figure 8. Medial aspect of human cortex A) Medial aspect of human case HCD with demarcations of areas established by von Economo. B) Medial aspect of human cortex provided by the atlas of von Economo & Koskinas (1925/20018)

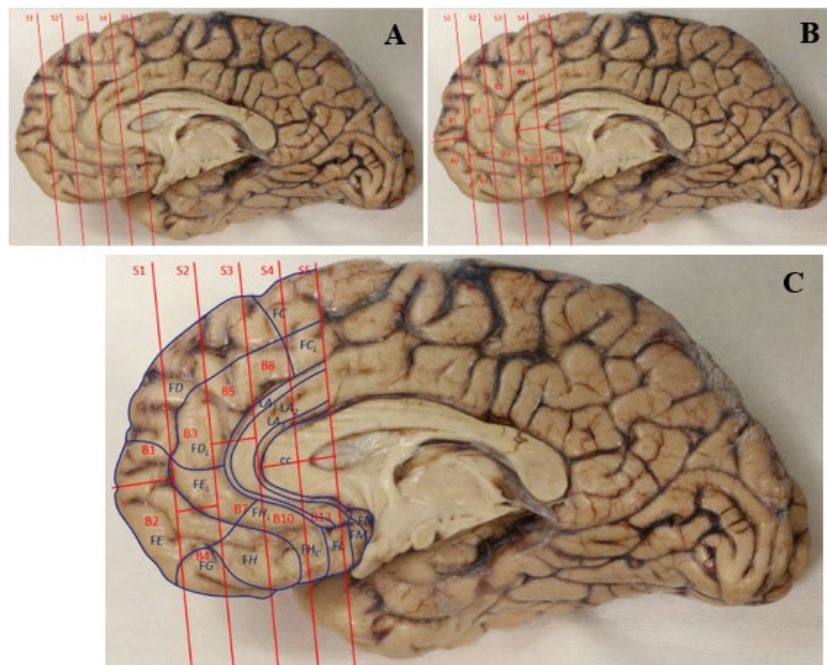


Figure 9. Processing and area parcellation of the medial aspect of human case HCD in accordance to the atlas of von Economo A) Medial aspect of human case HCD separated into 5 slabs of PFC. B) Medial aspect of human case HCD separated into multiple blocks within 5 slabs of PFC. C) Medial aspect of human case HCD separated into slabs and blocks with overlying von Economo area demarcations.

3.6 Quantitative Analysis

3.6.1 Plot Profiles

Each cortical column picture was edited in Adobe Photoshop to create an image that was in grayscale, inverted, and rotated 90 degrees counterclockwise. This was completed to orient each cortical column from the surface of the cortex (adjacent to layer I) on the left to the white matter (adjacent to layer VI) on the right. Images were then cropped for optimal visualization of layers I–VI with minimal white matter or open space. These sections were then analyzed for plot profile in ImageJ software, which was generated by ImageJ in scatterplot form

3.6.2 Mean Gray Values

After completion of the plot profile measurements in ImageJ, images were measured for mean gray value. Mean gray value, also known as optical density, was taken as a proxy of overall the cell density throughout the Nissl-stained cortical column.

3.6.3 Area Fractionation

After obtaining the mean gray value measurements in ImageJ, these images were thresholded. In the thresholded black and white view, white background represented neuropil while neurons and glia were labeled in black. Measurements were taken of these thresholded images to yield area fractionation of each cortical area. Area fractionation data was used to determine relative prominence of layers III and V in each cortical area based on the density of cells, while mean gray value was used to determine optical densities.

3.6.4 Mean Pyramidal Neuron Sizes and Externopyramidization

To compare data between the VE areas and human case HCD pictures, one cortical column picture of human case HCD was chosen to best represent the prefrontal VE areas (n=31). Utilizing ImageJ, four squares measuring 2.25 in^2 were placed on these cortical areas with two boxes in both layers III and V. These squares, or counting frames, were consistent in every cortical column picture. Next, the area fraction occupied by cells was obtained by thresholding the image and measuring the area fraction within each counting frame. Then, the images were restored from threshold to original Nissl-stained cortical areas, and the number of pyramidal neurons were counted per counting frame. Strict inclusion criteria were utilized to identify pyramidal neurons: 1) pyramidal neurons must have an approximate triangular shape; 2) pyramidal neurons must have a visible nucleolus; and 3) pyramidal neurons must have a visible apical dendrite. The apical dendrite qualification was made because apical dendrites are discernable in Nissl-stains, compared to basal dendrites, and the existence of two basal dendrites with absence of an apical dendrite could suggest the neurons were instead fusiform or basket shaped interneurons. The collected data for area fractionation and neurons counted were averaged per layer, and a mean neuron size (in^2) was calculated per layer. The mean neuron size in layer III was then divided by the mean neuron size in layer V to create a ratio externopyramidization. If this ratio of pyramidal neuron sizes in layers III:V showed a value larger than 1.0, this meant that the larger pyramidal neuron sizes were found in layer III. Conversely, if pyramidal neuron sizes in layers III:V showed a value less than 1.0, this meant that the larger pyramidal neuron sizes were found in layer V.

3.6.5 Non-metric Multidimensional Scaling

Non-metric Multidimensional Scaling (NMDS) allows for visualization of shared similarities within high dimensional data. Given the HCD-VE dataset (n=31), six features were utilized to perform NMDS, including: mean neuron size in LIII, mean neuron size in LV, averaged area fractionation for LIII, averaged area fractionation for LV, mean gray values, and plot profile in the form of a ratio of superficial to deep layers. These features were normalized, which reduced dimensionality of the data from six features to two dimensions while maintaining distances between the features. Two types of normalization were explored and represented in Figure 28A and 28B. Figure 28A shows normalization by maximum value in the dataset, while Figure 28B shows normalization by a z-scoring technique, which indicates how many standard deviations any given value is from the mean. Both of these normalization methods yielded similar results, as shown in Figures 28A and 28B.

CHAPTER 4: Results

4.1 Qualitative Analysis

4.1.1 Gross anatomy of the prefrontal cortex

The region of interest for this study was the PFC, which is the region of the frontal lobe that is rostral to precentral gyrus. The precentral gyrus is also known as the primary motor cortex, and the area immediately rostral to that is the premotor cortex, which serves as a transitional area between primary motor and prefrontal cortices. The primary motor cortex (area 4) is highlighted in red in Figure 10 (Mai *et al.* 2015), while the PFC consists of the regions in purple, pink, and tan.

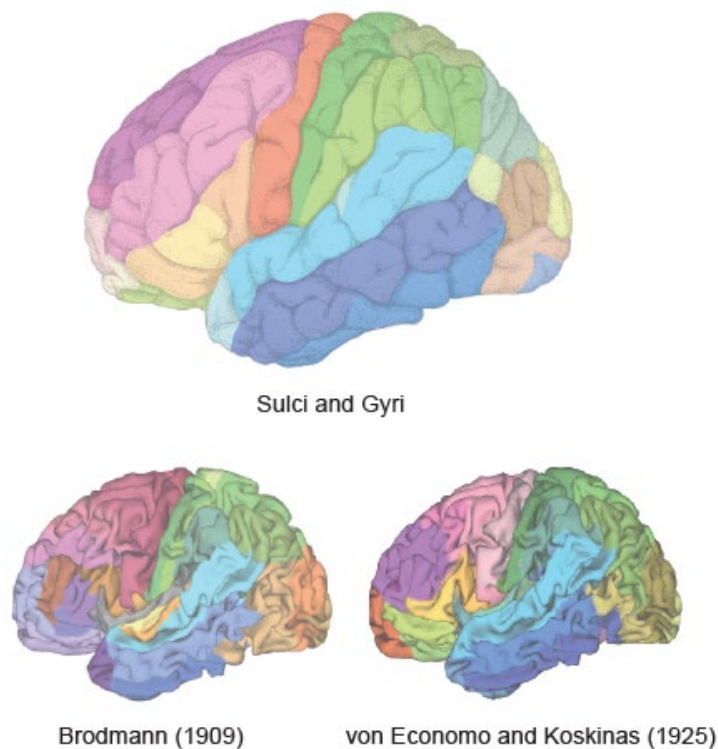


Figure 10. Diagrams of human cerebral cortex by sulci and gyri, Brodmann areas (1909), and von Economo/Koskinas areas (1925/2008), from Mai *et al.* (2015)

4.1.2 Blinded and unblinded classifications displayed gradients of cortical types throughout the human and monkey cortex

Cortical classifications in the human cortex were based on observations of inclusion criteria (summarized in Table 2) of Nissl-stained cortical areas. The Nissl stain is a purple-blue staining method that is utilized to visualize the nucleus and proximal cytoplasm of all neurons and glia in a given cortical column. Space unoccupied by purple-blue neurons or glia in a Nissl-stained cortical areas of tissue consists of axons and dendrites, otherwise known as neuropil. Based on Nissl stains, it was expected to be able to observe characteristics that would distinguish one cortical type from another. The presence of layer IV in a Nissl-stained tissue was seen as an area of small, granule-like neurons between superficial and deep layers. The relative prominence of superficial versus deep layers in a Nissl-stained tissue was visualized by density of neurons and glia and layer thickness of superficial or deep layers. The largest pyramidal neurons in a Nissl-stained tissue was a very evident feature, as these neurons were stained darkly in either layer III or V. The differentiation of layers V–VI in a Nissl-stained tissue was noted as differentiation of deep layers into sublayers Va, Vb, VIa, and VIb in more elaborate cortical types. Finally, the state of the boundary between layers I–II in Nissl-stained tissues was observed to be either irregular and wavering or a sharp and distinctive boundary between a layer I (which has few Nissl-stained neurons or glia) and layer II (which is densely populated by Nissl-stained neurons and glia).

Plates from the atlas of von Economo and Koskinas (1925/20018) were initially examined with blinding for cortical area, which ensured no bias in cortical type

classifications. Of note, this blinded study was similarly performed by researchers Bailey and von Bonin (1951), who reported that brain areas could not be distinguished from one another solely based on cytoarchitectonic criteria (Zilles & Amunts 2010). However, the present blinded and unblinded classification method showed that this was not the case for cortical types across different cortical areas. Cortical types showed distinctive and consistent characteristics of inclusion criteria across multiple cortical areas and lobes of the brain. These plates of the von Economo and Koskinas atlas (1925/2008) were re-examined without the blinding for cortical area to ensure assigned cortical types made topological sense. Blinded cortical type classifications were either identical to or nearly identical to the unblinded classification. The minimal corrections that were made were due to juxtaposed cortical types, which was consistent with the fact that laminar differentiation is observed in a gradual, sweeping gradient throughout the cortex. To re-examine these plates, limbic areas juxtaposed to the hippocampus (allocortex) were examined first. After limbic areas, eulaminate and koniocortical areas were examined. This showed a gradient of laminar differentiation from least elaborated to most elaborate, with the presence of layer IV increasing with every cortical type. The koniocortical area that was examined in this study was the primary motor region (area 4), which demonstrated the presence of a strong layer IV (García-Cabezas & Barbas 2014).

Results of these unblinded classifications of the plates of the atlas of von Economo and Koskinas (1925/2008) are summarized area in Tables 4–9, which are stratified by lobe. Tables 4 and 5 contain shaded rows that represent the VE areas that were present in the prefrontal human case HCD. Whenever appropriate, these VE areas

were further parcellated into one of four orientations of the cortex: medial, lateral, central, or ventral. Table 10 summarizes these cortical type classifications. There were a large number of eulaminar types (n=28 for eulaminar II; n= 31 for eulaminar I), a small number of limbic cortical types (n=18 for dysgranular; n=12 for agranular), a smaller number of koniocortices (n=11). Of note, the tables for the ‘Hippocampal (inferior limbic) lobe’ were not included in the cortical type analysis, as these classifications were entirely consistent with allocortex and not neocortex.

<u>Abbr.</u>	<u>Cortical Area</u>	<u>Plate #</u>	<u>Corresponding Brodmann Area</u>	<u>Cortical Type Classification</u>
FA	Precentral area	-	4	Koniocortex/ Primary motor**
FA γ	Giant pyramidal precentral area	1, 2, 3, 4, 66	4	Koniocortex/ Primary motor
FAop	Precentral area in operculum	-	4	Koniocortex/ Primary motor**
FAB	<i>Transitional Area</i>	5	-	Eulaminar II/ Premotor II
FB	Agranular frontal area	6, 7, 8	6, 8, 9	Eulaminar I/ Premotor I
FBop	Agranular frontal area in operculum		6	Eulaminar I/ Premotor I
FB(C)	<i>Transitional Area</i>	9	-	Eulaminar II/ Premotor II
FB(C)op	<i>Transitional Area</i>	10	-	Eulaminar I/ Premotor I
FBCop	<i>Transitional Area</i>	11	-	Eulaminar I/ Premotor I
*FC	Intermediate frontal area	12, 13	6, 8, 32	Eulaminar I/ Premotor I
FCL	Intermedio-limbic frontal area	17	32	Dysgranular

<i>FCBm</i>	Broca's area (magno-cellular agranular intermediate frontal area)	14, 15	44	Eulamine II/ Premotor II
<i>FCI</i>	Intermediate frontal area at the beginning of the insula	-	8	Eulamine I**
<i>FCop</i>	Opercular intermediate frontal area	16	8	Eulamine I
<i>FC(D)op</i>	<i>Transitional Area</i>	16	-	Eulamine I
<i>FC(D)</i>	<i>Transitional Area</i>	18	-	Eulamine I
<i>FDC</i>	<i>Transitional Area</i>	20	-	Eulamine I
<i>*FD</i>	Granular frontal area	24	9, 32, 46	Eulamine II
<i>*FDm</i>	Magno-cellular granular frontal area	19, 21, 23	9	Eulamine I/II
<i>FDm (C)</i>	<i>Transitional Area</i>	19	-	Eulamine II
<i>FDm (E)</i>	<i>Transitional Area</i>	21	-	Eulamine I
<i>FDm/FDp</i>	<i>Transitional Area</i>	23	-	Eulamine I
<i>*FDp</i>	Parvicellular granular frontal area	22, 23	9, 10, 11, 12	Eulamine I/II
<i>*FDop</i>	Granular frontal area in operculum	16	9, 10, 11, 12	Eulamine I
<i>*FDL</i>	Limbic granular frontal area	26	32	Eulamine I
<i>*FDΔ</i>	Middle granular frontal area	27	8, 9, 46	Eulamine II
<i>*FDΓ</i>	Triangular granular frontal area	28, 29, 30	45	Eulamine II
<i>*FE</i>	Frontopolar area	31	10, 32	Eulamine I/II
<i>*FEL</i>	Limbic frontopolar area	-	32	Eulamine I
<i>*FFg</i>	Granular orbital area	32	13, 47	Eulamine I

*FFa	Agranular orbital area	33	13, 47	Dysgranular
*FF ϕ	Pretriangular orbital area	34	47	Eulaminate I
*FG	Area of straight gyrus (area recta)	35	11	Eulaminate I
FGi	Internal straight area	-	-	Eulaminate I**
*FH	Prefrontal area	37	11, 12, 13a, 14, 25, 32	Eulaminate I
*FHL'	Parolfactory prefrontal area	39	11, 12, 13a, 14, 25, 32	Dysgranular
*FHL	Limbic prefrontal area	38	32	Dysgranular
*FJ	Frontoinsular area	42, 44	16	Agranular/ Dysgranular
FK	Frontal piriform area	-	16	Agranular/ Dysgranular**
FL1	Primary parolfactory area	39, 40	14, 25	Dysgranular
FL2	Secondary parolfactory area	40	14, 25	Agranular
FL3	Tertiary parolfactory area	40	14, 25	Agranular
FM	Geniculate area	40	25	Agranular
FMI	Geniculate area of olfactory triangle	-	25	Agranular**
FN	Precommissural area	40	-	Allocortex

Table 4. Cortical Type Classifications in the Frontal Lobe by von Economo/

Koskinas Areas

**Cortical areas used in adjacent comparison to HCD cortical areas.*

***Cortical type classifications were derived based on neighboring classifications and topological organization of the cortex, as no picture was available in the atlas of von Economo & Koskinas (1925/20018).*

<u>Abbr.</u>	<u>Cortical Area</u>	<u>Plate #</u>	<u>Corresponding Brodmann Area</u>	<u>Cortical Type Classification</u>
*LA1	Precingulate agranular anterior limbic area	45	24, 33	Dysgranular
*LA2	Anterior cingulate agranular anterior limbic area	46	24	Agranular/ Dysgranular
*LA3	Cingulate agranular anterior limbic area limitans	47	24	Agranular
LB1	Anterior ultracingulate area	47	24, 33	Allocortex
LB2	Area of the indusium	47	24, 33	Allocortex
LC1	Dorsal posterior cingulate area	48	31	Eulaminar I
LC2	Ventral posterior cingulate area	49	23	Dysgranular
LC3	Posterior cingulate area limitans	50	33	Agranular
LD	Agranular retrosplenial area	52	30	Agranular
LE1	Superior retrosplenial area granulosa	52	29	Dysgranular
LE2	Inferior retrosplenial area granulosa	52	26, 29	Agranular
LF1	Posterior ultracingulate area	52	26	Allocortex
LF2	Ultracingulate area oblecta	52	26	Allocortex

Table 5. Cortical Type Classifications in the Limbic Lobe by von Economo/

Koskinas Areas

**Cortical areas used in adjacent comparison to HCD cortical areas.*

***Cortical type classifications were derived based on neighboring classifications and topological organization of the cortex, as no picture was available in the atlas of von Economo & Koskinas (1925/20018).*

<u>Abbr.</u>	<u>Cortical Area</u>	<u>Plate #</u>	<u>Corresponding Brodmann Area</u>	<u>Cortical Type Classification</u>
IA1	Dorsal precentral insular area	53	14	Dysgranular
IA2	Ventral precentral insular area	54, 55	14	Dysgranular
IA2(B)	<i>Transitional Area</i>	55	-	Dysgranular
IB	Postcentral insular area	55, 56	13	Eulaminar I
IBT	Postcentral insular area at temporal entrance	57	13	Eulaminar I
IC	Orbito-insular area	58	15	Agranular/ Dysgranular
ID	Piriform insular area	-	16	Agranular/ Dysgranular**

Table 6. Cortical Type Classifications in the Insular Lobe by von Economo/

Koskinas Areas

***Cortical type classifications were derived based on neighboring classifications and topological organization of the cortex, as no picture was available in the atlas of von Economo & Koskinas (1925/20018).*

<u>Abbr.</u>	<u>Cortical Area</u>	<u>Plate #</u>	<u>Corresponding Brodmann Area</u>	<u>Cortical Type Classification</u>
<i>PA1</i>	Giant pyramidal postcentral area	59	3a	Eulaminar II
<i>PA2</i>	Giant pyramidal postparacentral area	59, 66, 67	3a, 5	Eulaminar II
<i>PB2</i>	Oral postcentral area simplex	60, 61	3, 3b	Koniocortex
<i>PB1</i>	Oral postcentral area granulosa	59, 60, 61, 62	3, 3b	Koniocortex
<i>PC</i>	Intermediate postcentral area	63	1, 2	Eulaminar II
<i>PCγ</i>	<i>Transitional Area</i>	64	-	Eulaminar II/ Koniocortex
<i>PD</i>	Caudal postcentral area	65	2, 5a	Eulaminar II
<i>P(D)E</i>	Superior parietal area (transition parietal postcentral area)	65	2, 40	Eulaminar II
<i>PEm</i>	Magnocellular superior parietal area	68, 69	5, 7, 7a	Eulaminar II
<i>PEp</i>	Parvicellular superior parietal area	70	5b, 7, 7b	Eulaminar II
<i>PEγ</i>	Giant pyramidal posterior superior parietal area	71	5b, 7, 7b	Eulaminar II
<i>PF</i>	Supramarginal area	72, 73, 74	7b, 22, 40	Eulaminar I/II
<i>PFt</i>	Tenuicortical supramarginal area	75	7b, 22, 40	Eulaminar I
<i>PFop</i>	Opercular supramarginal area	77	Opercular	Eulaminar II
<i>PFcm</i>	(Posterior) magnocellular supramarginal area	75	40	Eulaminar I
<i>PG</i>	Angular area	76	7a, 39	Eulaminar I
<i>PHP</i>	Basal (temporooccipital) parietal area at parietal entrance	78	37	Eulaminar I/II
<i>PHT</i>	Basal (temporooccipital) parietal area at temporal entrance	80	37	Eulaminar I

<i>PHO</i>	Basal (temporooccipital) parietal area at occipital entrance	79	37	Eulaminate II
------------	--	----	----	---------------

Table 7. Cortical Type Classifications in the Parietal Lobe by von Economo/

Koskinas Areas

<u>Abbr.</u>	<u>Cortical Area</u>	<u>Plate #</u>	<u>Corresponding Brodmann Area</u>	<u>Cortical Type Classification</u>
<i>OA2</i>	Anterior peristriate area	81	19	Eulaminate II
<i>OAI</i>	Posterior peristriate area	82, 83	19	Eulaminate II
<i>OAm</i>	Magnocellular peristriate area	81	19	Eulaminate II
<i>OB</i>	Parastriate area	83, 84, 85, 87	18	Eulaminate II
<i>OBy</i>	Giant pyramidal parastriate boundary	85, 86, 87	17/18 border	Koniocortex
<i>OBo</i>	Maculae granulosae of parastriate area	-	18	Eulaminate II**
<i>OC</i>	Striate area (granulosa)	85, 86, 87, 88	17	Koniocortex

Table 8. Cortical Type Classifications in the Occipital Lobe by von Economo/

Koskinas Areas

***Cortical type classifications were derived based on neighboring classifications and topological organization of the cortex, as no picture was available in the atlas of von Economo & Koskinas (1925/20018)*

<u>Abbr.</u>	<u>Cortical Area</u>	<u>Plate #</u>	<u>Corresponding Brodmann Area</u>	<u>Cortical Type Classification</u>
TA1	Posterior superior temporal area	88, 89, 92	22	Eulaminar II
TA2	Anterior superior temporal area	-	22	Eulaminar I**
TB	Magnocellular supratemporal area simplex	93	22, 42	Eulaminar II/ Koniocortex
TC	Supratemporal area granulosa	94	41	Koniocortex
TD	Intercalated supratemporal area	95	22, 42	Koniocortex
TE1	Middle temporal area proper	89, 90	21, 37	Eulaminar I
TE2	Inferior temporal area proper	91	20, 21	Eulaminar I
TF	Fusiform area	96	36	Eulaminar I
TH	Hippocampotemporal area	108	35, 36	Agranular
TH α	Agranular hippocampotemporal area	-	35	Agranular**
TG	Temporopolar area	97	Anterior 35–36, 38, 52	Dysgranular
TG α	Agranular temporopolar area	98, 99	Anterior 35–36, 38, 52	Agranular
TJ	Temporal piriform area	98	16	Agranular
TK	Posterior area of substantia perforata	-	-	Agranular/ Dysgranular**

Table 9. Cortical Type Classifications in the Temporal Lobe by von Economo/

Koskinas Areas

***Cortical type classifications were derived based on neighboring classifications and topological organization of the cortex, as no picture was available in the atlas of von Economo & Koskinas (1925/20018).*

<u>Char-acter-istics</u>	CORTICAL TYPES*					<i>Total</i>
	<i>LIMBIC</i>		<i>EULAMINATE</i>		<i>PRIMARY CORTICAL AREAS</i>	
	<u>A-granular</u>	<u>Dys-granular</u>	<u>Eulamine I/ Premotor I</u>	<u>Eulamine II/ Premotor II</u>	<u>Koniocortex/ Primary Motor</u>	
Total	12	18	31	28	11	100

Table 10. Summary of assigned cortical types in the human cerebral cortex from the atlas of von Economo/Koskinas

**Allocortex (n=5) were excluded from summary, as it is not neocortex.*

Following the completion of cortical type analysis of the atlas of von Economo & Koskinas (1925/20018), this cortical type analysis using Table 2 for classification was applied to the total number of pictures taken (n=482) of the PFC of human case HCD. These classifications are summarized in Table 11. Of the pictures that were utilized in this study (n=311), meaning they did not fall under any exclusion criteria, there were a large number of eulamine cortical types (n=114 for eulamine II; n=167 for eulamine I) and a small number of limbic cortical types (n=21 for dysgranular; n=9 for agranular).

Cortical type classifications were found to be translational across species. A small number of motor areas were examined in this study, as the PFC is located immediately rostral to the border of the premotor region. The premotor region lies rostral to the motor cortex in the precentral gyrus and contains cortical types that are similar in laminar differentiation to eulamine I and II in human tissue. The primary motor cortex was identified in human tissue as koniocortex for its high level of elaboration, high density of neurons in the superficial layers, and presence of Betz cells in layer V. However, motor

areas observed in the rhesus macaque tissue did not have a visible layer IV. Therefore, Table 2 and 3 show characteristics of differential laminarity in human and monkey cortical types, respectively. The five laminar features used for cortical type classifications of humans and rhesus macaques were identical.

Pictures of the cerebral cortex of rhesus macaque case RAR (n=106) were analyzed with cortical type classifications using Table 3. Table 12 summarizes these classifications. There were a large number of limbic cortical types (n=43 for dysgranular; n=12 for agranular), a small number of eulaminate types (n=23 for eulaminate II; n= 25 for eulaminate I), a smaller number of koniocortices (n=3). When comparing human tissue to rhesus macaque tissue, it is evident that the ratio of eulaminate types to limbic types is quite higher in the human compared to the rhesus macaque. This difference between species is shown in Figure 11. Figure 11A shows cortical types in the PFC of human case HCD (n=482), while Figure 11B compares the cortical types in the cerebral cortices of human (n=100) and rhesus macaque (n=106). This suggests that while cortical types are conserved between the two species, a larger number of eulaminate areas are seen in humans.

<u>Characteristics</u>	CORTICAL TYPES					<i>Total</i>	<i>%</i>
	<i>LIMBIC</i>		<i>EULAMINATE</i>		<i>PRIMARY CORTICAL AREAS</i>		
	<u>A-granular</u>	<u>Dys-granular</u>	<u>Eulamine I/ Premotor I</u>	<u>Eulamine II/ Premotor II</u>	<u>Konio-cortex/ Primary Motor</u>		
Total	15	44	257	166	0	482	100
Used	9	21	167	114	0	311	64.5
Unused	6	23	90	52	0	171	35.5

Table 11. Summary of assigned cortical types in the PFC of human case HCD

<u>Characteristics</u>	CORTICAL TYPES					<i>Total</i>
	<i>LIMBIC</i>		<i>EULAMINATE</i>		<i>PRIMARY CORTICAL AREAS</i>	
	<u>A-granular</u>	<u>Dys-granular</u>	<u>Eulamine I/ Premotor I</u>	<u>Eulamine II/ Premotor II</u>	<u>Koniocortex/ Primary Motor</u>	
Total	12	43	25	23	3	106

Table 12. Summary of assigned cortical types in cerebral cortex of rhesus macaque case RAR

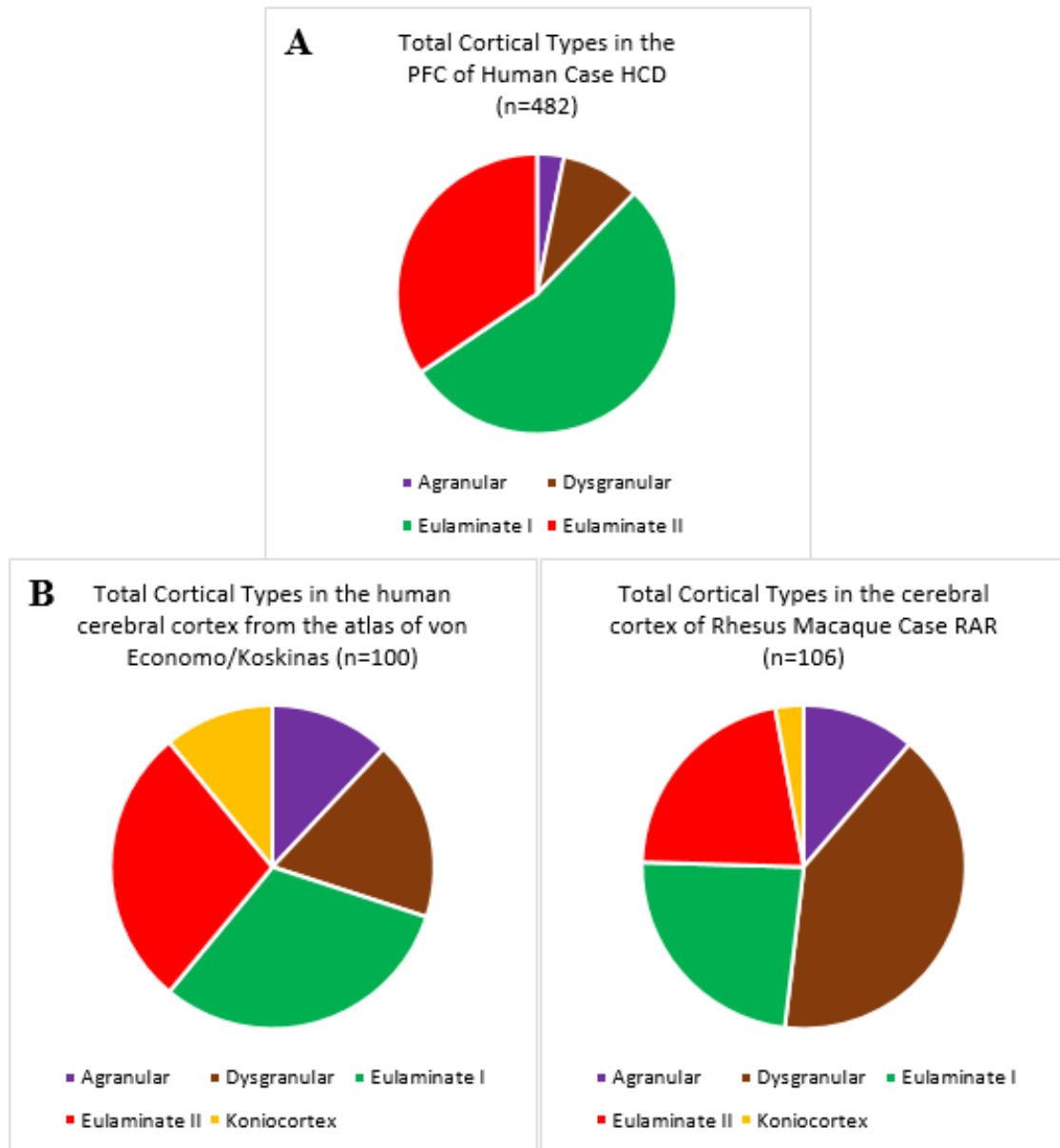


Figure 11. Comparison of cortical type distribution in human and rhesus macaque cortices **A)** Prefrontal cortex cortical types in human case HCD (n=482). **B)** Cerebral cortex cortical types in human photomicrographs of the atlas of von Economo/Koskinas (n=100); Cerebral cortex cortical types in rhesus macaque case RAR (n=106).

4.1.3 SMI-32 Neurofilament Staining

To reinforce the concept of differing laminarity across cortical types, SMI-32 neurofilament staining was utilized via immunohistochemistry. SMI-32 was utilized because it labels the soma and proximal dendritic processes of pyramidal neurons in deep layer III and superficial layer V, but does not stain any neurons in layer IV. This allowed for clear evidence of several distinguishable features of interest to this study, including layer IV as a non-labeled band, as well as relative prominence of either layer III or V. For example, in agranular regions, it would be expected to observe prominent deep layers and no presence of layer IV. Conversely, eulaminate II areas would be expected to have prominent superficial layers and presence of a well-defined layer IV. Figure 12 shows the four different cortical types labeled with SMI-32 juxtaposed with Nissl tissue of the corresponding cortical area. These columns were obtained in the same block 10 of the PFC of human case HCD, which emphasizes the existence of gradients in laminar differentiation across the cortex. This shows that the cortex is not as homogeneous as some textbooks suggest; instead, there is an inherent heterogeneous gradient of cortical types throughout the cortex.

The agranular cortical type in a SMI-32 stained tissue has very little staining with a few neurons that are lightly labeled in the deep layers. The dysgranular cortical type in a SMI-32 stained tissue has a bit more staining visible in the deep layers, particularly layer V. The eulaminate I cortical type in a SMI-32 stained tissue has increasingly darker staining with visible neurons in deep superficial layer III and superficial layer V. Finally, the eulaminate II cortical type in a SMI-32 stained tissue has a thick band of very dark

and punctate pyramidal neurons labeled in layer III, as well as clear sublayers in deep layers V and VI.

The empty space visualized in the SMI-32 stained tissue is neuropil and unlabeled neurons. Another stain that has been utilized in prior studies is a myelin stain, which labels intracortical myelin and increases in density from limbic to eulaminate areas (García-Cabezas *et al.* 2019). This trend is the opposite of the trend seen with SMI-32, and can be regarded as a stain for neuropil space within a cortical column. While a myelin stain was not performed in this study, it shows great promise as a visual contrast to the SMI-32 staining technique when examining cortical types.

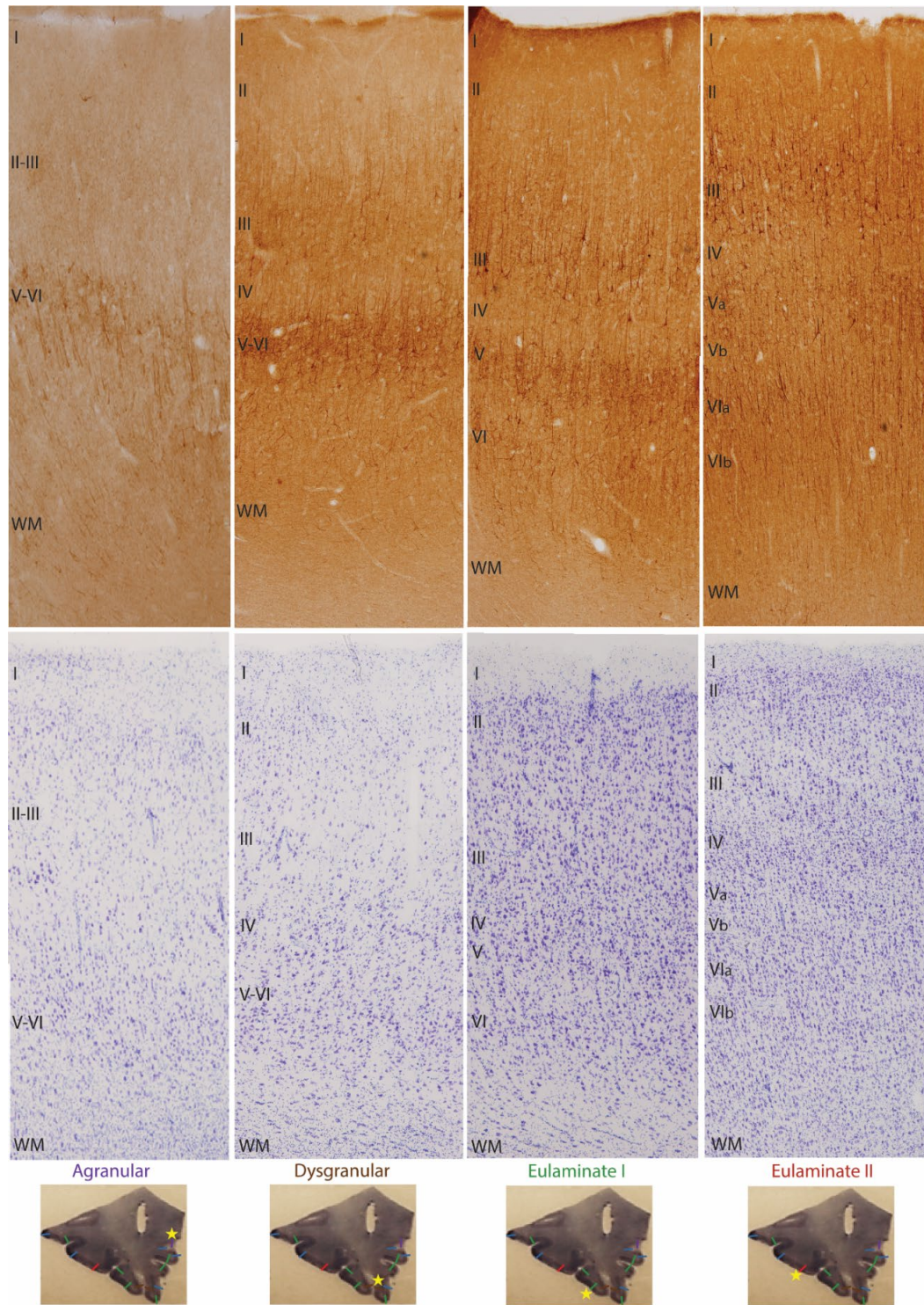


Figure 12. Comparison of SMI-32 and Nissl staining of the four cortical type in posterior block 10 of human case HCD

4.2 Quantitative Analysis

4.2.1 Plot Profiles

Plot profiles of cortical columns were taken to show varying laminarity throughout each layer, from the surface of the cortex to the white matter. The plot profile measurement was designed to show the number of neurons and glia that were present in each layer of the Nissl-stained cortex. Layers that were closer to the surface of the cortex were noted as superficial layers I, II, and upper III, layers that were in the middle were noted as deep part of layer III and layer IV, and layers that were closer to the white matter were noted as deep layers V and VI. It was predicted that limbic cortical types, such as agranular and dysgranular, would have a gradual rise in slope and a peak closer to the white matter, which would represent the prominent deep layers that are characteristic of limbic cortical types. Conversely, it was predicted that eulaminate cortical types, such as eulaminate I and II, would have a lower density of neurons and glia near the white matter, but have a steep rise in slope with a peak closer to the surface of the cortex, which would represent the prominent superficial layers that are characteristic of eulaminate cortical types.

The plot profiles of the four cortical types were averaged and normalized for length, with results shown in Figure 13. Eulaminate I and dysgranular plot profile trends were consistent with what was expected from their respective cortical types. The plot profile slope of eulaminate I cortical areas showed an even U-shaped curve in the middle, between the surface of the cortex and the white matter, suggesting that there is equal prominence between layers III and V. The plot profile slope of dysgranular cortical areas

showed a gradual rise in slope with a raised plateau closer to the white matter, suggesting a small relative prominence of deep layers V–VI.

Figure 13 also shows that eulaminate II and agranular plot profile trends were not consistent with expectations of their cortical type characteristics. There was anticipation for these two plot profile trends to be opposite of one another, with eulaminate II demonstrating a peak closer to the surface of the cortex and agranular demonstrating a peak closer to the white matter. Instead, these two plot profile trends have plateau-like characteristics. It is hypothesized that these plot profile trends appear this way due to differences in layer thickness. Plot profile measurements were continuous measurements of the cortical column and did not include additional information about the thickness of the layers. For instance, the eulaminate cortical type is expected to have a thick and prominent layer III compared to layer V, while the agranular cortical type is expected to have a thick and prominent layer V compared to layer III. Due to the fact that the layers were not labeled during this quantitative measurement, these two opposite sides of the cortical type spectrum, eulaminate II and agranular, were distorted during normalization of lengths. According to this interpretation of the data, the plateau-like curves of the averaged trend lines occurred because the eulaminate II plot profile trendline was shifted to the right while the agranular plot profile trendline was shifted to the left.

Plot profile data for the HCD-VE data was represented as a ratio of neurons and glia in superficial to deep layers, which is shown in Figure 14. Representing this plot profile data as a ratio from superficial to deep layers accounts for the differences in layer thickness. While eulaminate I and II showed some variability, the general trend showed a

gradual increase in neurons and glia in the superficial layers from limbic to eulaminate types.

Plot profile measurements were also obtained for the PFC plates of the atlas of von Economo. These plates, which were displayed to show varying cortical types throughout the cortex of the human brain, often showed transitional regions between two cortical types. Therefore, transitional areas were included in the analysis of these plates, with nine different types: koniocortex/primary motor, eulaminate II/premotor II, eulaminate II, eulaminate I/II, eulaminate I/premotor I, eulaminate I, dysgranular, dysgranular/agranular, and agranular. Results are summarized in Figure 15 and are found to generally obey the same trends. In summary, plot profiles show an estimate of the number of neurons and glia present throughout the layers of the cortex. These results show that the complexity of laminar differentiation can be appreciated with this method, and should be used as supplemental support to qualitatively-determined cortical types.

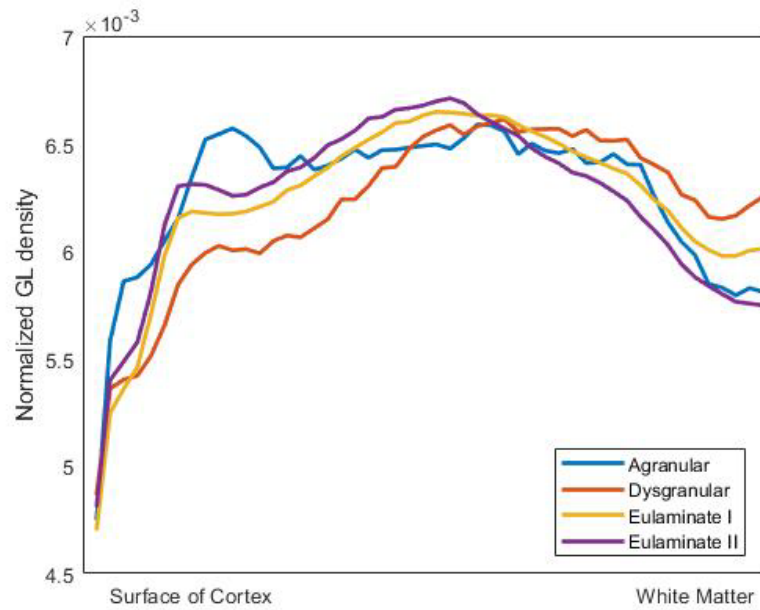


Figure 13. Representation of plot profile trends of the four cortical types spanning from the surface of the cortex to white matter in the prefrontal cortex of human case HCD

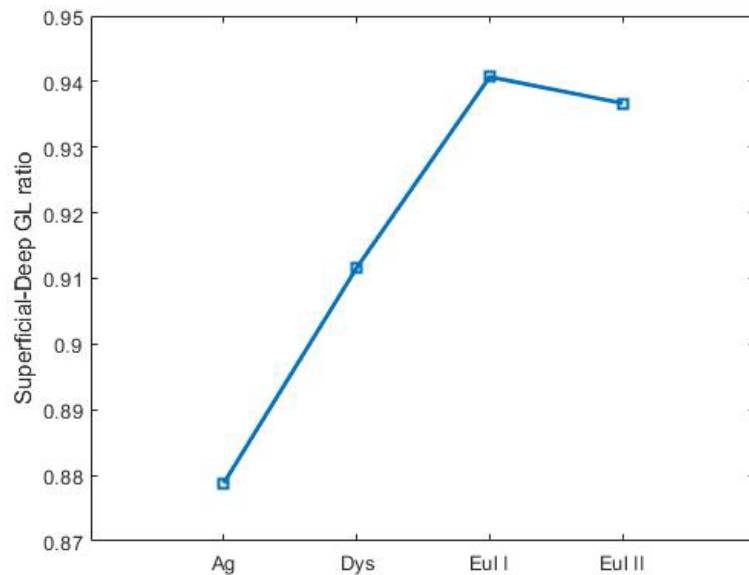


Figure 14. Averaged ratio of the upper half of plot profiles to the lower half of plot profiles, stratified by cortical type

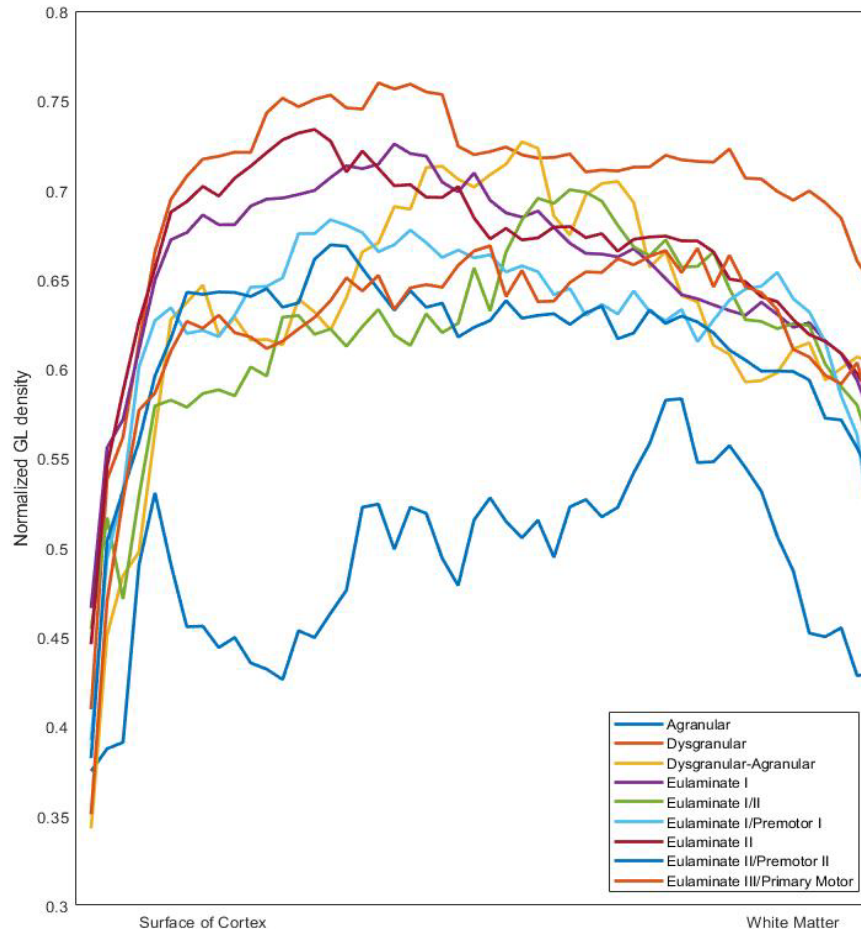


Figure 15. Representation of plot profile trends of the cortical types spanning from the surface of the cortex to white matter of the prefrontal cortex in atlas of von Economo & Koskinas (1925/2018)

4.2.2 Mean Gray Values

Mean gray values were obtained to assess the optical density of cells throughout the cortical column. This measurement was a type of signal labeling that was also dependent on background. Figures 16 and 17 show mean gray value data for all used cortical areas (n=311) separated by orientation (medial, central, ventral, and lateral) for eulaminate II and I cortical types respectively. Figures 18 and 19 show mean gray value

data for all used cortical areas (n=311) separated by orientation (medial, ventral) for dysgranular and agranular cortical types respectively. Results showed that mean gray value is not a very helpful measurement in determining cortical type; as values show no discernable trends. For this reason and additional hypotheses that warrant more examination, it seems that mean gray values simply cannot substitute the human eye when laminar differentiation is involved.

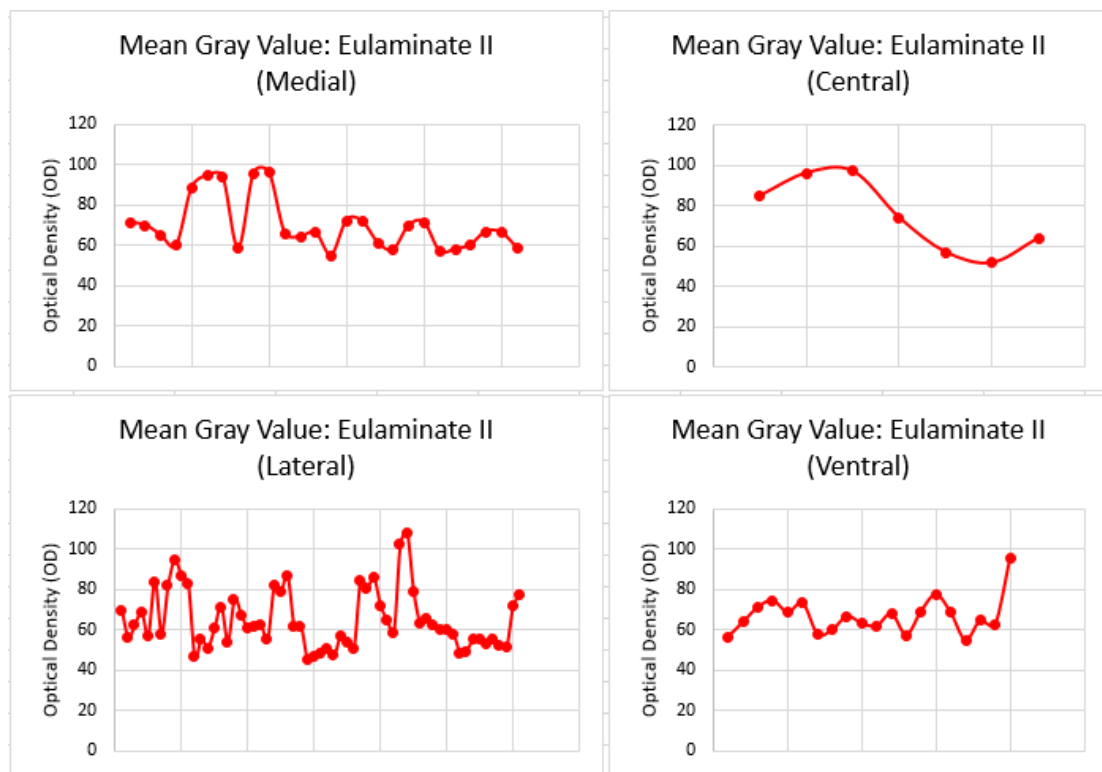


Figure 16. Mean gray values for the Eulaminate II cortical type separated by orientations of medial, central, lateral, and ventral

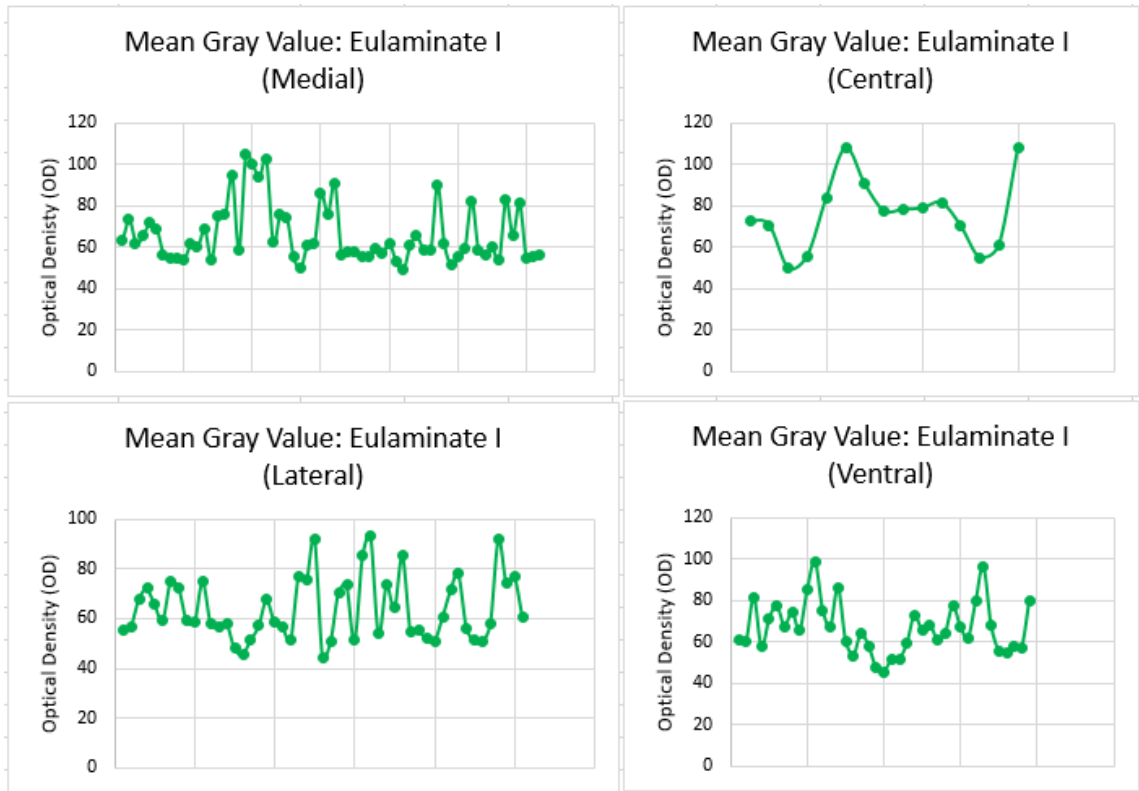


Figure 17. Mean gray values for the Eulaminat I cortical type separated by orientations of medial, central, lateral, and ventral

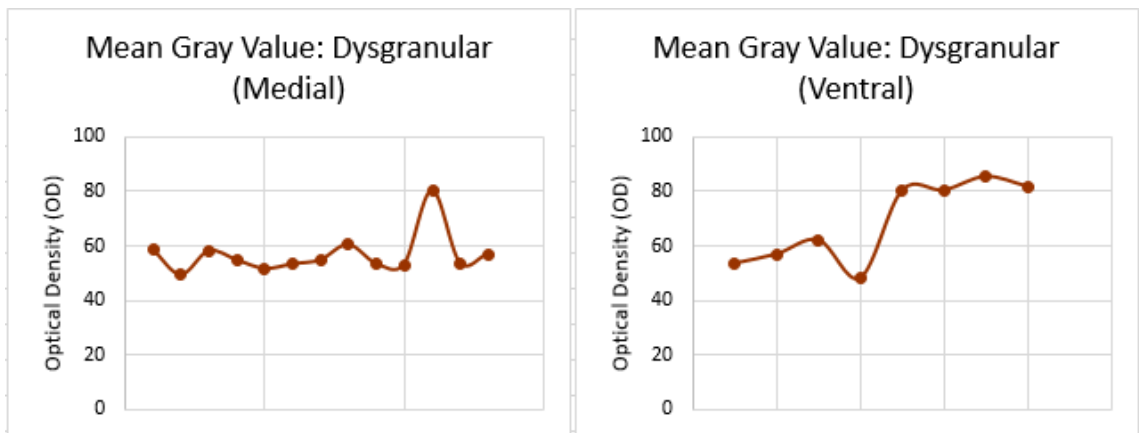


Figure 18. Mean gray values for the Dysgranular cortical type separated by orientations of medial and ventral

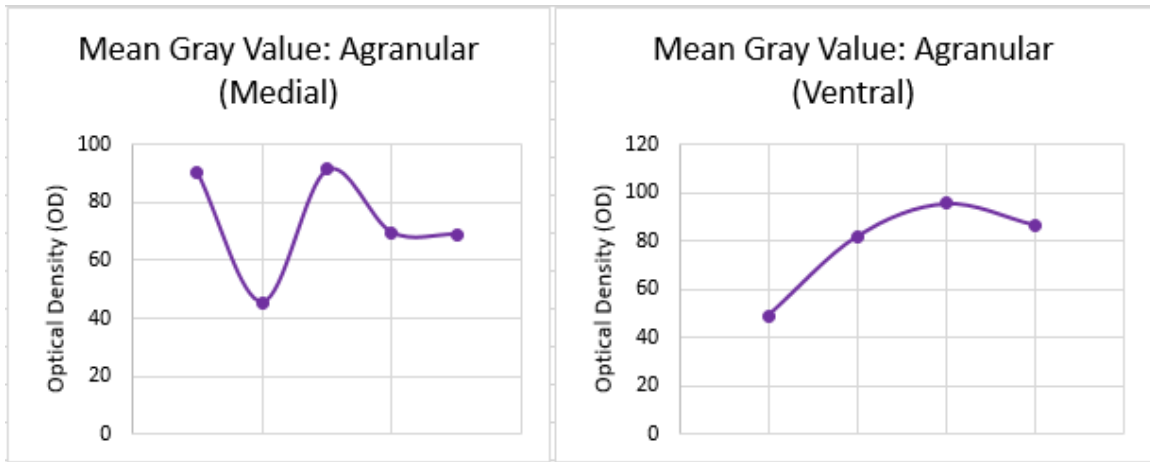


Figure 19. Mean gray values for the Agranular cortical type separated by orientations of medial and ventral

4.2.3 Area Fractionation

Area fractionation data showed differences in neuron density between layers III and V. Figure 20 shows averaged area fractionation data stratified by cortical type, with results that were consistent with expectations. Based on criteria for cortical type classifications, as summarized in Table 2, the eulaminate II type was expected to show relative prominence in layer III; the eulaminate I type was expected to show equally relative prominence in layers III and V; and dysgranular and agranular types were expected to show relative prominence in layer V.

Figures 21 and 22 show area fractionation data for all used cortical areas (n=311) separated by orientation (medial, central, ventral, and lateral) for eulaminate II and I cortical types respectively. Figures 23 and 24 show area fractionation data for all used cortical areas (n=311) separated by orientation (medial, ventral) for dysgranular and agranular cortical types respectively. These figures reiterate that trends show some

individual variance but were primarily consistent with cortical type predictions of relative prominence in layers III and V.

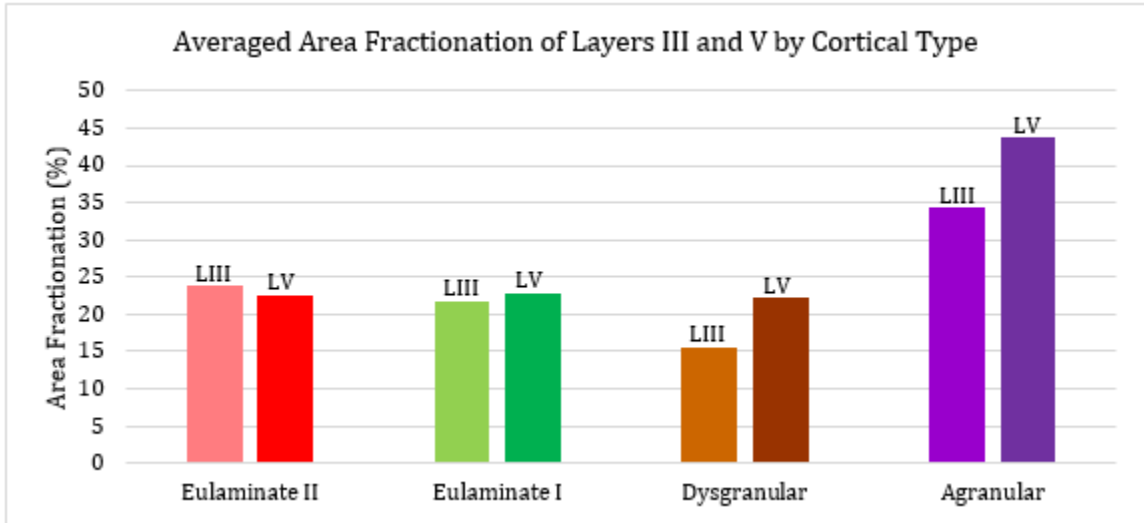


Figure 20. Averaged area fractionation for layers III and V in four cortical types

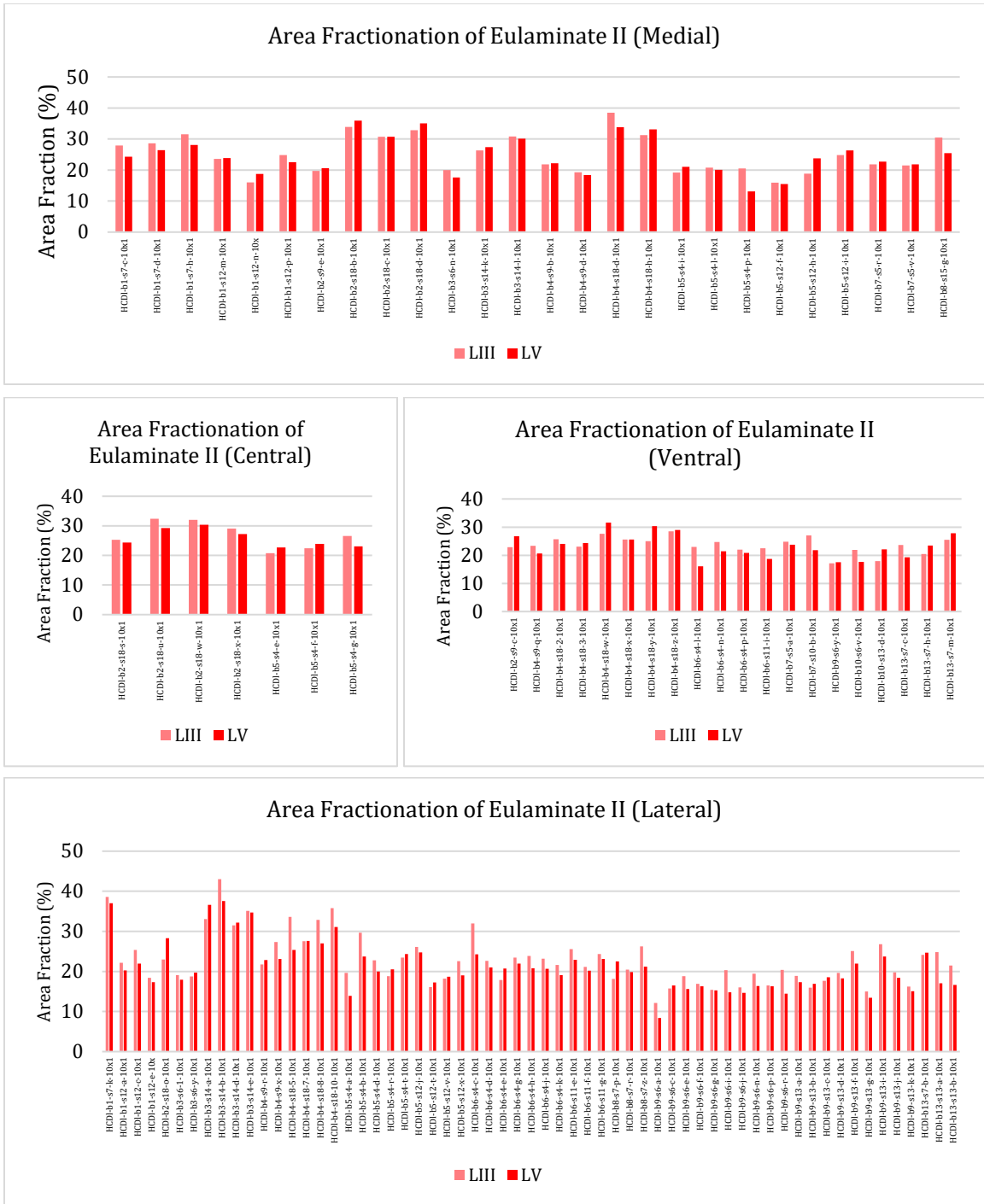


Figure 21. Area fractionation for layers III and V in the Eulaminate II cortical type separated by orientations of medial, central, ventral, and lateral

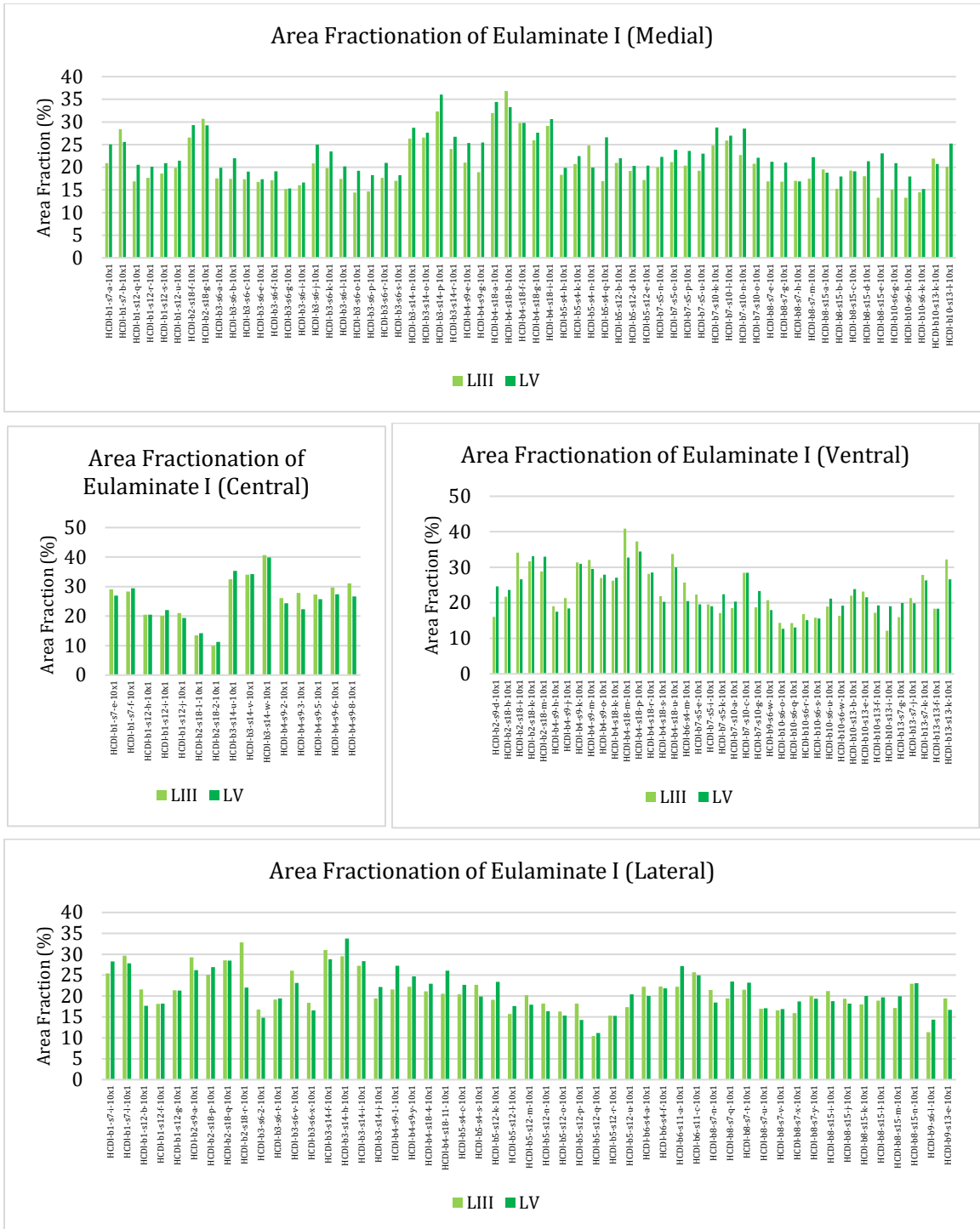


Figure 22. Area fractionation for layers III and V in the Eulaminate I cortical type separated by orientations of medial, central, ventral, and lateral

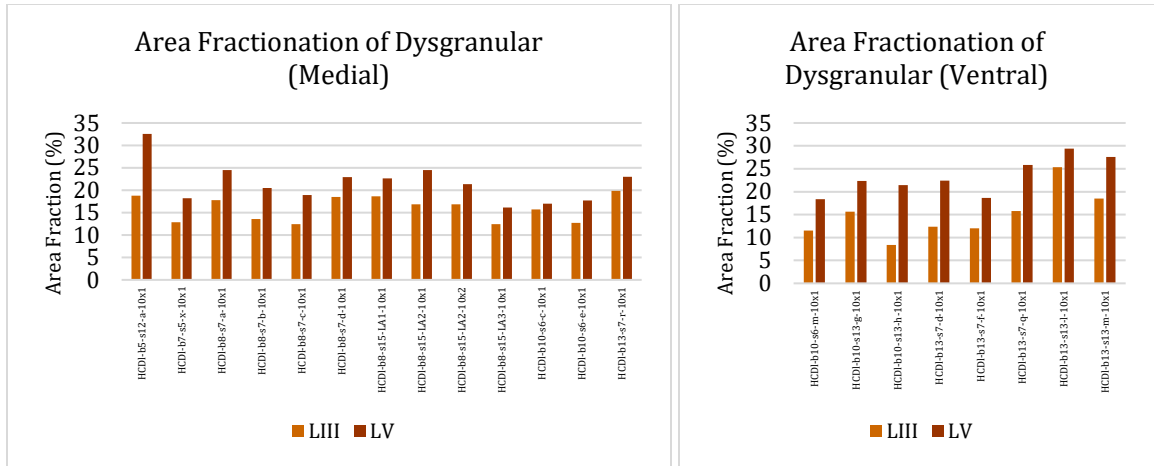


Figure 23. Area fractionation for layers III and V in the Dysgranular cortical type separated by orientations of medial and ventral

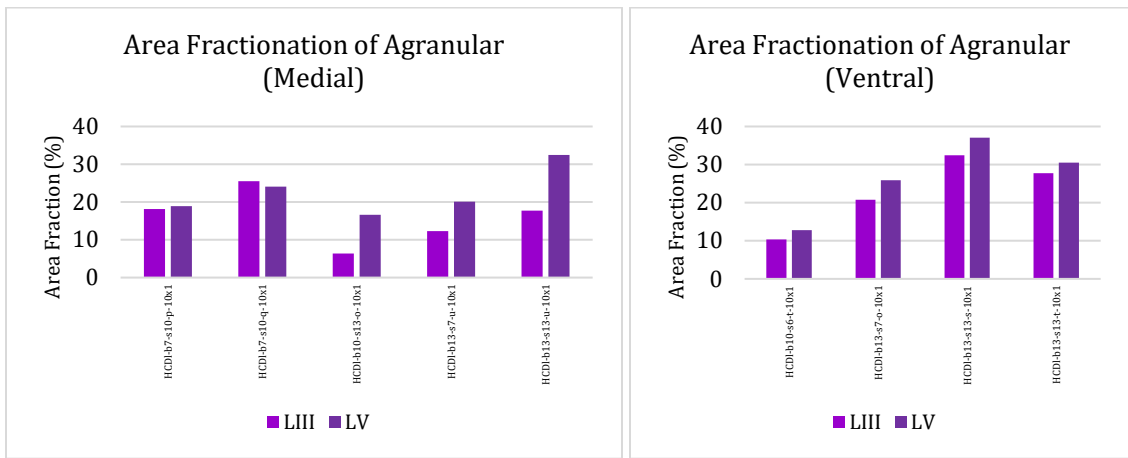
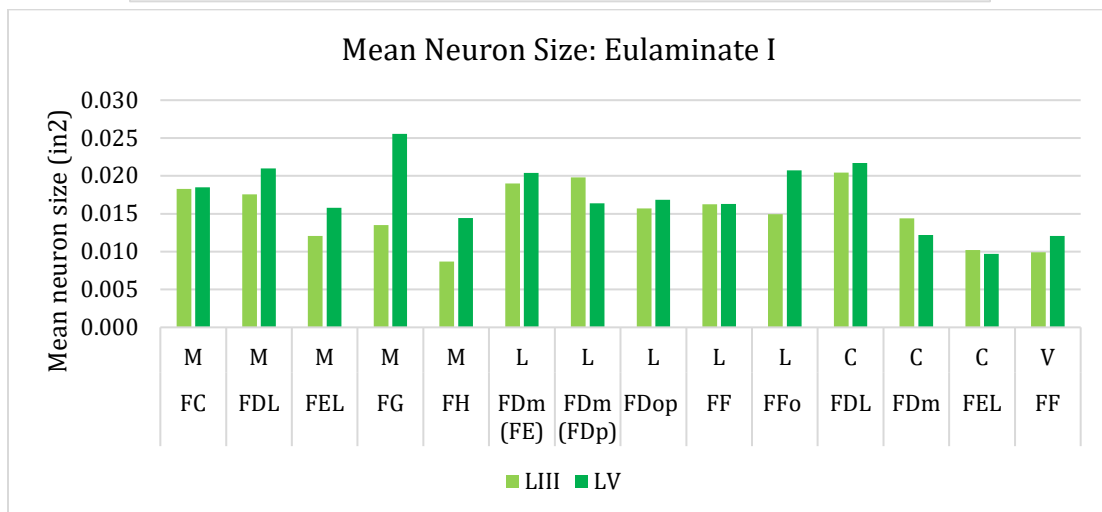
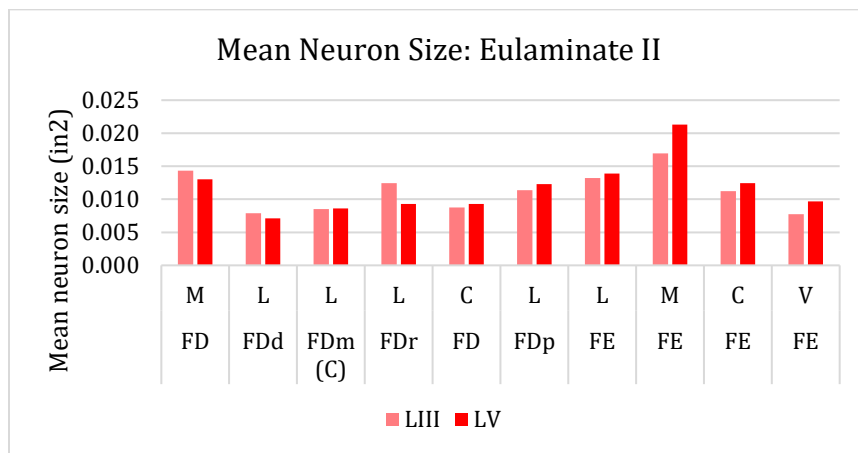


Figure 24. Area fractionation for layers III and V in the Agranular cortical type separated by orientations of medial and ventral

4.2.4 Mean Pyramidal Neuron Sizes and Ratio in Layers III and V

Mean neuron sizes for the comparative HCD-VE cortical areas (n=31) were taken to show localization of largest pyramidal neurons in layers III versus V. This data was much more consistent with predictions for limbic areas, with mean neuron sizes undisputedly

larger in layer V of dysgranular and agranular regions. Mean neuron size in eulaminate areas, however, was not always consistent with predicted trends. Eulaminate areas, including eulaminate II and eulaminate I, were predicted to show larger neuron sizes in layer III in comparison to layer V. Results of this measurement, shown in Figure 25, showed a large variability between mean neuron sizes in eulaminate cortical types, making this measurement a suboptimal method of predicting cortical type. Confounding factors that could be responsible for these inconsistent results include over-representation of small pyramidal neurons, over-representation of non-pyramidal neurons, or under-representation of large pyramidal neurons.



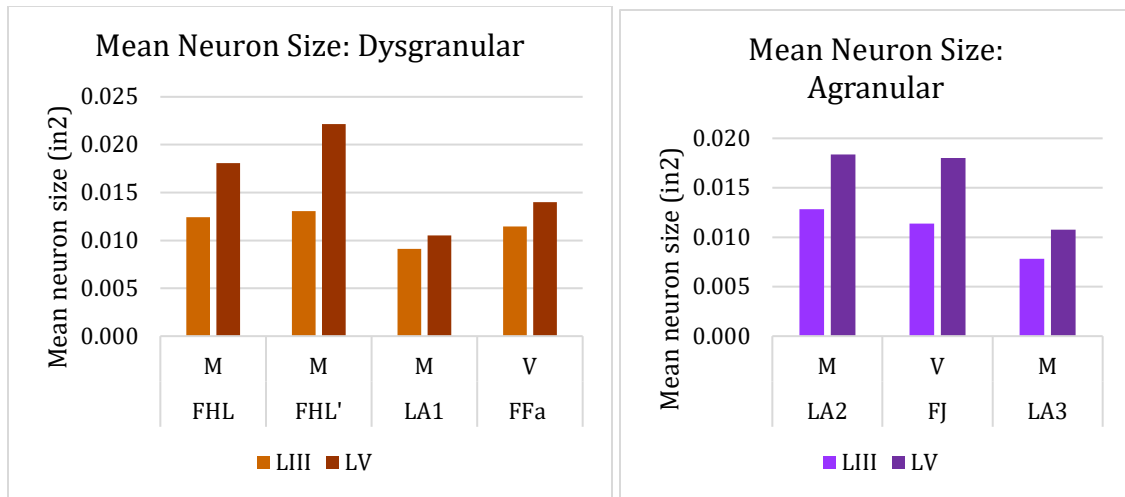


Figure 25. Area fractionation for layers III and V in the varying cortical types separated by von Economo areas

The externopyramidization, or ratio of mean neuron sizes in layers III:V, of cortical areas of HCD-VE (n=31) were mostly consistent with predictions. Eulaminate II was predicted to have values above 1.0, indicating the presence of larger pyramidal neurons in layer III versus layer V. Eulaminate I was expected to show variability above and below 1.0. Dysgranular and agranular were predicted to have values below 1.0, indicating the presence of larger pyramidal neurons in layer V. Figures 26 and 27 show externopyramidization results for HCD-VE across cortical types overall and averaged, respectively. While limbic cortical types were consistent with expectations, eulaminate areas are again observed to be variable. Overall, this data shows consistency with predicted outcomes, but shows that mean neuron size in layers III and V cannot by itself predict cortical type, as estimated in this study.

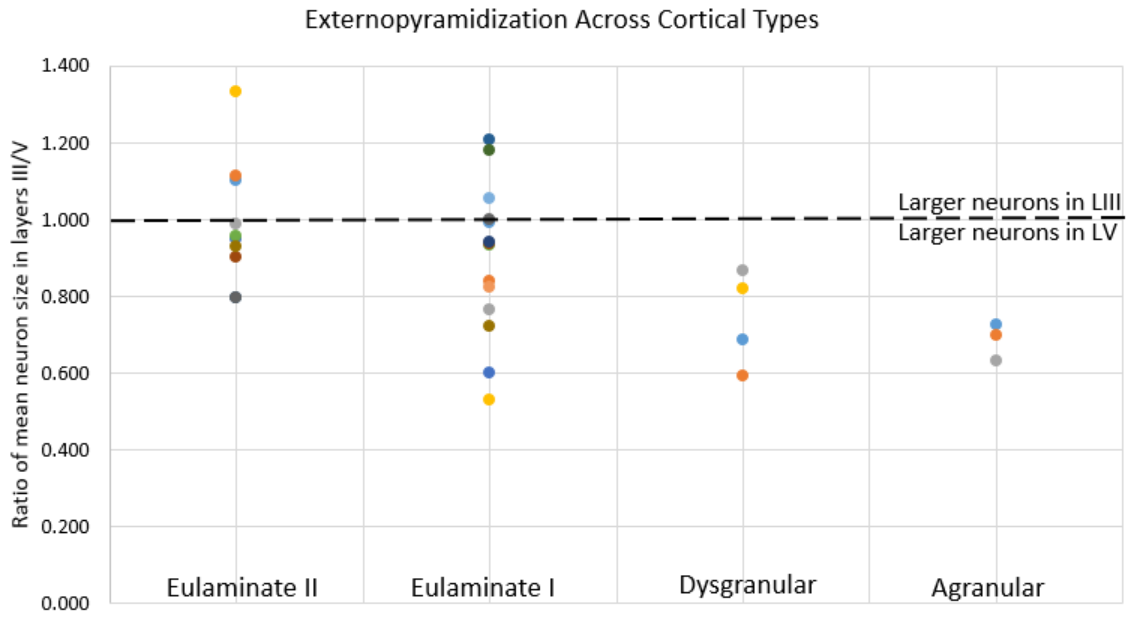


Figure 26. Externopyramidization showing ratio of layers III to V in compared cortical areas stratified by cortical type

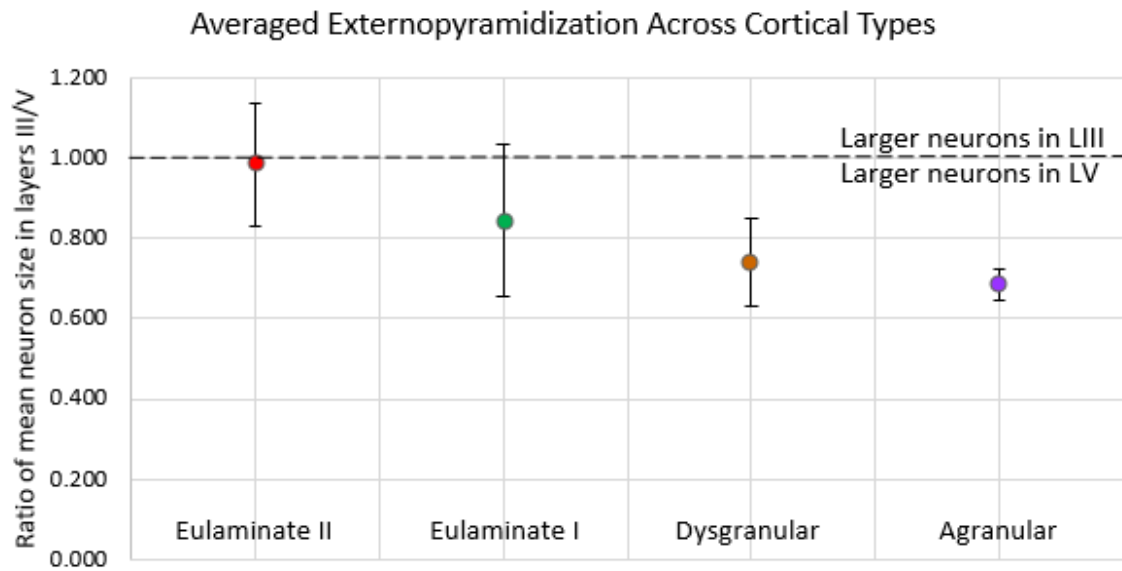


Figure 27. Averaged externopyramidization showing ratio of layers III to V in compared cortical areas stratified by cortical type

4.2.5 Non-metric Multidimensional Scaling

NMDS analysis was performed in order to observe any trends that may exist, based on a few features that are reduced into two dimensions. Figure 28A and B show two different types of normalization that were performed during the NMDS analysis. Figure 28A shows normalization by maximum value amongst the different datasets. A trend can be observed in Figure 28A from the top left corner down to the bottom right corner, showing limbic (agranular in red; dysgranular in green) to eulaminate (eulaminate I in blue; eulaminate II in purple). Figure 28B shows normalization by the z-scoring technique, also known as standard scoring. A trend can also be observed from the bottom to the top of the graph, with more limbic types on the bottom and more eulaminate types on the top. Neither of these plots show any jumps in laminarity; instead, both plots show that cortical types obey a gradual gradient throughout the PFC. Taken together, these trends show that there are shared similarities amongst the different cortical types, and that laminar differentiation is observed in a gradual pattern.

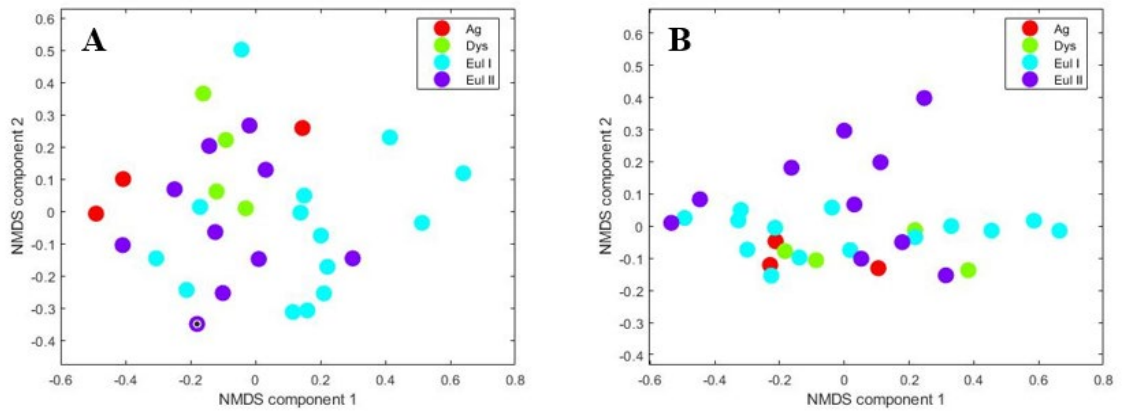


Figure 28. NMDS analysis of HCD-VE demonstrates expected trends by two methods of normalization A) Normalization by the maximum value of the datasets B) Normalization by z-scoring

CHAPTER FIVE: Discussion

This study has provided a method of parcellating cortical regions into three broad categories in the human and rhesus macaque, from least elaborate to most elaborate types: limbic, eulaminate, and koniocortex. These three overarching categories have subdivisions, with agranular and dysgranular subdivisions of limbic, eulaminate I and II subdivisions of eulaminate, and koniocortex representing the primary areas of the cortex.

While the existence of gradients in cortical type across different cortical areas is strongly supported by prior studies [reviewed in (García-Cabezas *et al.* 2019)], how cortical type divisions are determined is regarded as a pure subjective measure. This study employed quantitative measures to identify differences between the established cortical types to lessen the subjectivity of cortical type classification. When establishing the four main cortical types (agranular, dysgranular, eulaminate I, and eulaminate II), this study sought to avoid the occurrence of over-parcellation that was suggested by Bailey and von Bonin (1951) and Puelles (2019). Results of this study avoided over-parcellation, through the use of the algorithm for differing characteristics between cortical types (summarized in Table 2) that allowed determination of cortical type with less than 5% of variance amongst at least three experienced neuroanatomists in the laboratory that this study was conducted.

Efforts were made in this study to automate the process of cortical type classification, so that individuals who are not experts in neuroanatomy could classify cortical types. To prove that cortical type classifications based on Nissl staining are reproducible and are not purely subjective, quantitative analysis was performed. Plot

profile and area fractionation were shown to be the best representative measures of reported cortical type characteristics. Conversely, mean pyramidal neuron sizes and externopyramidization showed consistent trends in limbic types but not eulaminate types, which were more variable and heterogeneous than expected. In addition, mean gray value was seen as a near useless measure when determining cortical type, as the values were too dependent on background, which can be highly variable from one Nissl-stained section to another.

Overall, the quantitative results of this study showed undisputable trends of differences in laminar differentiation across the cortical types, with some measures more effective than others. Non-metric multi-dimensional scaling (NMDS) results showed that a combination of six different quantitative datasets, including mean neuron size in LIII, mean neuron size in LV, averaged area fractionation for LIII, averaged area fractionation for LV, mean gray values, and plot profile in the form of a ratio of superficial to deep layers. Results of NMDS showed a clear trendline of gradual laminar differences across cortical types, with no significant jumps observed.

A confounding factor of this study was the presence of blood vessels within the columns examined—some pictures contain large, sweeping blood vessels that would certainly interfere with this measure. In addition, a clear confounding factor is the variable darkness of Nissl-staining. Each block of post-mortem human tissue was processed one at a time, with the variable quantities of thionin blue permeating the tissues, as well as variable quantities of acetone during the dehydration process to remove excess thionin from the tissue. With consideration of these confounding factors in mind,

this study can be reproduced and improved in the future.

Our findings provide a framework for many future studies, including examination of properties that are linked to cortical types, such as epigenetics, synaptic plasticity, connections, pathologies, and evolution. The utilization of molecular markers would reveal the epigenetic landscape influencing laminar differentiation. Prior studies have shown that limbic cortical types have both high plasticity for the integration of new memories and learning, as well as high vulnerability for neurologic and psychiatric diseases like Alzheimer's disease (García-Cabezas *et al.* 2017). One study that could have been performed to represent plasticity would be myeloarchitectonic analysis to study the intracortical connections, as was initially demonstrated by Vogt & Vogt (1919). By utilizing a myelin stain, prior studies have shown that differences in cortical type can be observed (Zikopoulos *et al.* 2018), with increasing density of myelin from limbic to eulaminate areas (García-Cabezas *et al.* 2019). In addition, cortical type was shown to have translational characteristics between the rhesus macaque and human. This study showed that there were more eulaminate cortical types in the human than in the rhesus macaque. However, further quantitative studies should be performed on the rhesus macaque tissue to investigate how plot profile and area fractionation trends align with those of human.

Future studies should definitely include mention of functionality of the region of interest. While it is accepted that the PFC controls many of our executive functions, this study did not review the individual functional implications of each von Economo or Brodmann cortical area. Glasser *et al.* (2016) utilized a functional fMRI approach and

parcellated 180 total cortical areas, of which there were 51 prefrontal areas. In this study, there were 31 von Economo & Koskinas (1925/20018) areas that were applicable and related to the PFC of processed human case HCD. The varying number of cortical area parcellations is an important feature to be cautious of, for over- or under-parcellation of the human cortex could lead to misconceptions of functionality and plasticity in a clinical setting.

An interesting method to further explore and advance this field would be to create a scoring system for the cortical type classifications. This scoring system would be based off of the five cortical type characteristics, all of which are summarized in Table 2. Less elaborate cortical types (limbic) would have a lower scoring, while the more elaborate cortical types (eulaminate/koniocortex) would have a much higher scoring. This scoring system would bear much similarities to Table 2, and would be translational to cortices of mammals, including rat, rhesus macaque, and human. The goal of this approach would be to provide a more sweeping gradient of cortical types within the established five cortical types, as well as provide an undisputable algorithm for quantitative measurement of cortical types. This proposed scoring model is summarized in Table 13.

<u>Characteristics</u>	<u>1 Point</u>	<u>2 Points</u>	<u>3 Points</u>
Existence of Layer IV	Absent	Thin	Thick
Relative prominence of Superficial versus Deep Layers	Layers V–VI	Equal prominence in Layers II–III & Layers V–VI	Layers II–III
Largest pyramidal neurons	Layer V	Equal in Layers III and V	Layer III
Differentiation of Layers V–VI	None; Layers V–VI only	Yes; Presence of Layers V–VI	Yes; Presence of Sublayers Va/b & VIa/b
State of boundary between Layers I–II	Irregular	Sharp	Sharp and Defined

Table 13. Proposed scoring criteria for improved generalization of cortical type classifications

CHAPTER SIX: Conclusions

By integrating both qualitative and quantitative analysis in the study of laminar differentiation of the human cortex, this study has shown that there is a way to categorize and distinguish different cortical types throughout the PFC. The algorithm provided by this study allows for reproducible and accessible classification of cortical types using Nissl-stained tissue, which has not been successful prior to this study. Qualitative analysis by blinded and unblinded observation of Nissl-stained cortical columns in an established atlas and a processed post-mortem human brain revealed five cortical type characteristics that allow more objectivity in classification of cortical types. These cortical type characteristics could be used for the classification of cortical types in humans and rhesus macaques, which demonstrates evolutionary conservation of cortical types between human and rhesus macaque, with higher number of eulaminar cortical types to limbic cortical types in the human compared to rhesus macaque. An exhaustive analysis of human tissue led to a plethora of data to perform quantitative analysis upon, with plot profile and area fractionation measures showing the most promise in differentiating between cortical types, and mean gray values showing the least promise. Mean pyramidal neuron sizes and externopyramidization measures of comparison cortical columns HCD-VE showed consistent trends in limbic types and variable trends in eulaminar types. NMDS analysis of the six quantitative datasets showed a gradient of different cortical types, from the most limbic to most eulaminar types. This study was meant to set a foundation for future studies by providing a method of cortical type classification that is supported by both qualitative and quantitative measures.

BIBLIOGRAPHY

- Abbie, A.A. (1940) Cortical lamination in the monotremata. *Journal of Comparative Neurology*, **72**, 429–467.
- Abbie, A.A. (1942) Cortical lamination in a polyprotodont marsupial, *Perameles nasuta*. *Journal of Comparative Neurology* **76**, 509–536.
- Bailey, P. & von Bonin, G. (1951) *The Isocortex of Man*. University of Illinois Press, Urbana.
- Barbas, H. (1986) Pattern in the laminar origin of corticocortical connections. *Journal of Comparative Neurology*, **252**, 415–422.
- Barbas, H. & Rempel-Clower, N. (1997) Cortical structure predicts the pattern of corticocortical connections. *Cerebral Cortex*, **7**, 635–646.
- Brodmann, K. (1909/1999) *Brodmann's Localisation in the Cerebral Cortex*. Translated from German by Laurence J. Garey. Imperial College Press, London.
- Campbell, M. J. & Morrison, J. H. (1989) Monoclonal antibody to neurofilament protein (SMI-32) labels a subpopulation of pyramidal neurons in the human and monkey neocortex. *Journal of Comparative Neurology*, **282(2)**, 191–205.
- Dart, R.A. (1934) The dual structure of the neopallium: Its history and significance. *Journal of Anatomy*, **69**, 3–19.
- García-Cabezas, M. Á., & Barbas, H. (2014) Area 4 has layer IV in adult primates. *European Journal of Neuroscience*, **39(11)**, 1824–1834.
- García-Cabezas, M. Á., Joyce, M. K. P., John, Y. J., Zikopoulos, B., & Barbas, H. (2017) Mirror trends of plasticity and stability indicators in primate prefrontal cortex. *European Journal of Neuroscience*, **46(8)**, 2392–2405.
- García-Cabezas, M.A., Zikopoulos, B., and Barbas, H. (2019) The Structural Model: a theory linking connections, plasticity, pathology, development and evolution of the cerebral cortex. *Brain Structure and Function*, **224(3)**, 985–1008.
- Glasser, M.F., Coalson, T.S., Robinson, E.C., Hacker, C.D., Harwell, J., Yacoub, E., Ugurbil, K., Andersson, J., Beckmann, C.F., Jenkinson, M. and Smith, S.M. (2016) A multi-modal parcellation of human cerebral cortex. *Nature*, **536 (7615)**, 171.
- Mai, J. K., Majtanik, M., & Paxinos, G. (2015) *Atlas of the human brain*. Academic Press.

- Puelles, L. (2017) Comments on the updated tetrapartite pallium model in the mouse and chick, featuring a homologous claustrinsular complex. *Brain, Behavior, and Evaluation*, **90**(2), 171–189.
- Puelles, L., Alonso, A., García-Calero, E., & Martínez-de-la-Torre, M. (2019) Concentric ring topology of mammalian cortical sectors and relevance for patterning studies. *Journal of Comparative Neurology*, **527**(10), 1731–1752.
- Sanides, F. (1962) Architectonics of the human frontal lobe of the brain. With a demonstration of the principles of its formation as a reflection of phylogenetic differentiation of the cerebral cortex. *Monographien aus dem Gesamtgebiete der Neurologie Psychiatrie*, **98**, 1–201.
- Trutzer, I.M., García-Cabezas, M.A., & Zikopoulos, B. (2019) Postnatal development and maturation of layer 1 in the lateral prefrontal cortex and its disruption in autism. *Acta Neuropathologica Communications* **7**(1), 40.
- Vogt, C. & Vogt, O. (1919) Allgemeinere Ergebnisse unserer Hirnforschung. *Journal für Psychologie und Neurologie / Journal of Neurology and Psychology* **25**, 292–398.
- von Economo, C., & Koskinas, G.N. (1925/2008) *Atlas of cytoarchitectonics of the adult human cerebral cortex*. Translated from the German original, revised and edited with an Introduction and addition appendix material by L.C. Triarhou. Karger, Basel; New York.
- Zikopoulos, B., & Barbas, H. (2006) Prefrontal projections to the thalamic reticular nucleus form a unique circuit for attentional mechanisms. *Journal of Neuroscience*, **26**(28), 7348–7361.
- Zikopoulos, B., García-Cabezas, M. Á., & Barbas, H. (2018) Parallel trends in cortical gray and white matter architecture and connections in primates allow fine study of pathways in humans and reveal network disruptions in autism. *PLoS Biology*, **16**(2), e2004559.
- Zilles, K., & Amunts, K. (2010) Centenary of Brodmann's map—conception and fate. *Nature Reviews. Neuroscience* **11**(2), 139–145.

CURRICULUM VITAE

